Microgrids (Part II)
Microgrid Modeling and Control

GRA: Zixiao Ma
Advisor: Dr. Zhaoyu Wang
Department of Electrical and Computer Engineering
Iowa State University

Contents

- Dynamic Modeling of Microgirds
  - Background of Microgrids Modeling
  - Mathematical Modeling of Inverter-Dominated Microgrids
  - Reduced-Order Small-Signal Model of Inverter-Dominated Microgrids
- Microgrids Control: Primary and Secondary
  - Primary Control
    - Active Load Sharing
    - Droop Characteristic Techniques
    - Discussion of Primary Control Level Techniques
  - Secondary Control
    - Literature Review of Secondary Control
    - Distributed Cooperative Secondary Control of Microgrids Using Feedback Linearization

Background of Microgrids Modeling

- Microgrids as the main building blocks of smart grids are small scale power systems that facilitate the effective integration of distributed energy resources (DERs).
- In normal operation, the microgrid is connected to the main grid. In the event of disturbances, the microgrid disconnects from the main grid and goes to the islanded operation.
- In the islanded mode operation of a microgrid, a part of the distributed network becomes electrically separated from the main grid, while loads are supported by local DERs. Such DERs are typically power electronic based, making the full system complex to study.
- A detailed mathematical model of microgrids is important for stability analysis, optimization, simulation studies and controller design.

Mathematical Model of Microgrid

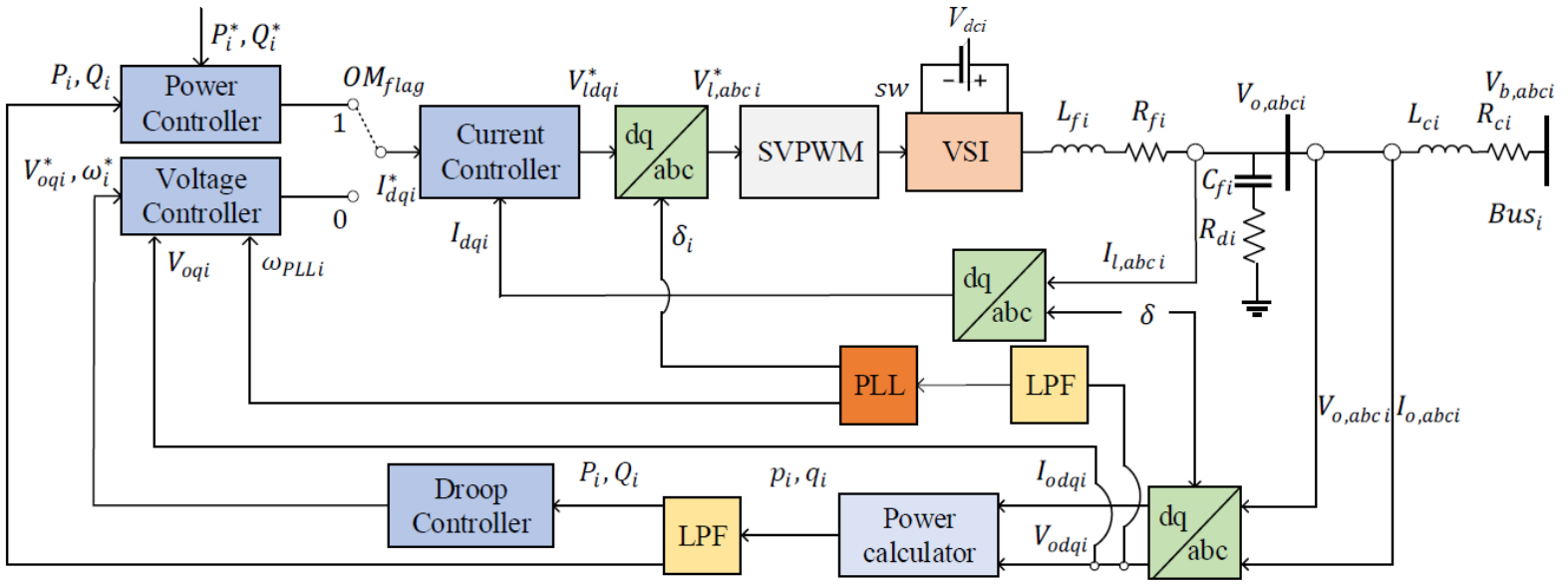

Fig. 1. The diagram of VSI-based DER and controller block.

- $OM_{flag} = 1$: the microgrid is operated in grid-tied mode
- $OM_{flag} = 0$: the microgrid is operated in islanded mode

Mathematical Model of Microgrid

a) Average Power Calculation: The generated active and reactive power can be calculated using the transformed output voltage V_{odq} and current I_{odq}. The average power generated by the inverter is

$$p = \left(v_{od}i_{od} + v_{oq}i_{oq}\right), \quad (1a)$$

$$q = \left(v_{oq}i_{od} - v_{od}i_{oq}\right). \quad (1b)$$

Using a low-pass filter (LPF) with the corner frequency ω_c,we can obtain the filtered instantaneous powers as follows,

$$\dot{P} = -P\omega_c + \omega_c\left(v_{od}i_{od} + v_{oq}i_{oq}\right), \quad (2a)$$

$$\dot{Q} = -Q\omega_c + \omega_c\left(v_{oq}i_{od} - v_{od}i_{oq}\right). \quad (2b)$$

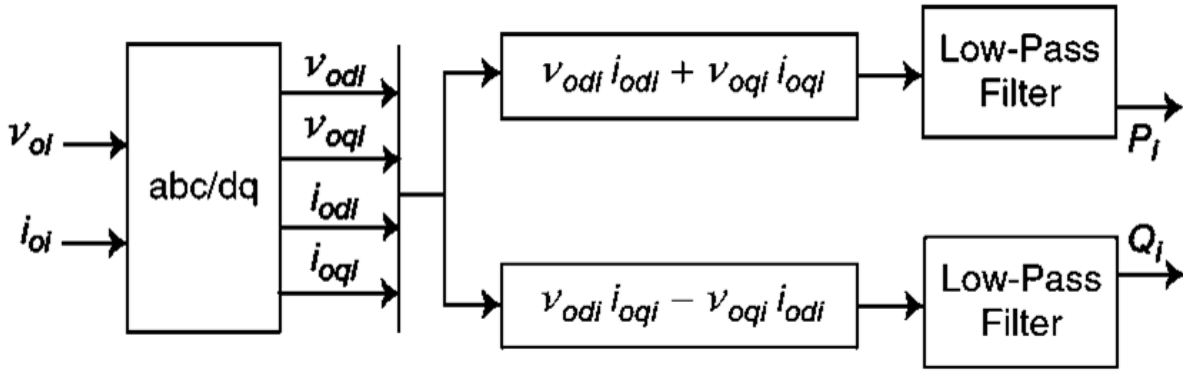

Fig. 2. The diagram power calculator.

Mathematical Model of Microgrid

b) Phase Locked Loop: The phase lock loop (PLL) is used to measure the actual frequency of the system. According to [1], the PLL input is the *d*-axis component of the voltage measured across the filter capacitor (Fig. 4).

The mathematical model of PLL is represented as follows,

$$\dot{v}_{odf} = \omega_{cPLL} v_{od} - \omega_{cPLL} v_{odf}, \tag{3a}$$

$$\dot{\varphi}_{PLL} = -v_{odf}. \tag{3b}$$

In grid-tied mode, the inverter output phase is synchronized to the main grid using PLL, therefore the derivative of phase angle δ is set to ω_{PLL}:

$$\dot{\delta} = \omega_{PLL} = 377 - k_{p,PLL} v_{odf} + k_{i,PLL} \varphi_{PLL}. \tag{4}$$

In islanded mode, the phase angle of the first inverter can be arbitrarily set as the reference for the other inverters:

$$\dot{\delta}_i = \omega_{PLL1} - \omega_{PLLi} \quad i = 1, \ldots, n. \tag{5}$$

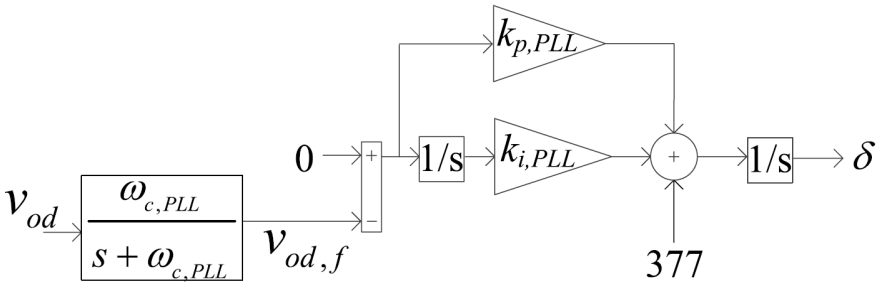

Fig. 3. The diagram of PLL used for DER.

[1] M. Rasheduzzaman, J. A. Mueller, and J. W. Kimball, "An accurate small-signal model of inverter-dominated islanded microgrids using dq reference frame," IEEE J. Emerg. Sel. Topics Power Electron., vol. 2, no. 4, pp. 1070–1080, Dec. 2014.

Mathematical Model of Microgrid

c) Power Controller: In grid-tied mode, the output power of DER is regulated by the power controller using PI control method. The input references are the commanded real and reactive powers:

$$\dot{\varphi}_P = P - P^*, \tag{6a}$$
$$i_{lq}^* = k_{i,pq}\varphi_P + K_{p,pq}\dot{\varphi}_P, \tag{6b}$$
$$\dot{\varphi}_Q = Q - Q^*, \tag{6c}$$
$$i_{ld}^* = k_{i,pq}\varphi_Q + K_{p,pq}\dot{\varphi}_Q. \tag{6d}$$

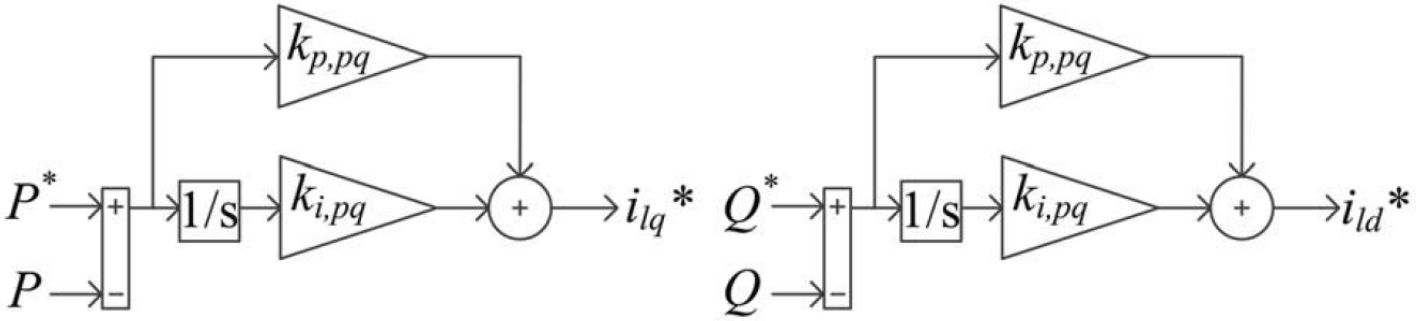

Fig. 4. The diagram of power controller PLL used for DER.

Mathematical Model of Microgrid

d) Droop Controllers: In grid-connected mode, the inverter's output voltage is set by the grid voltage magnitude. The PLL ensures proper tracking of grid phase so that inverter output remains synchronized to the grid. In islanded mode, a DER has no reference inputs from the main grid. Therefore, it must generate its only voltage and frequency references using droop controllers as follows,

$$\omega^* = \omega_n - mP, \tag{7a}$$

$$v_{oq}^* = v_{oq,n} - nQ. \tag{7b}$$

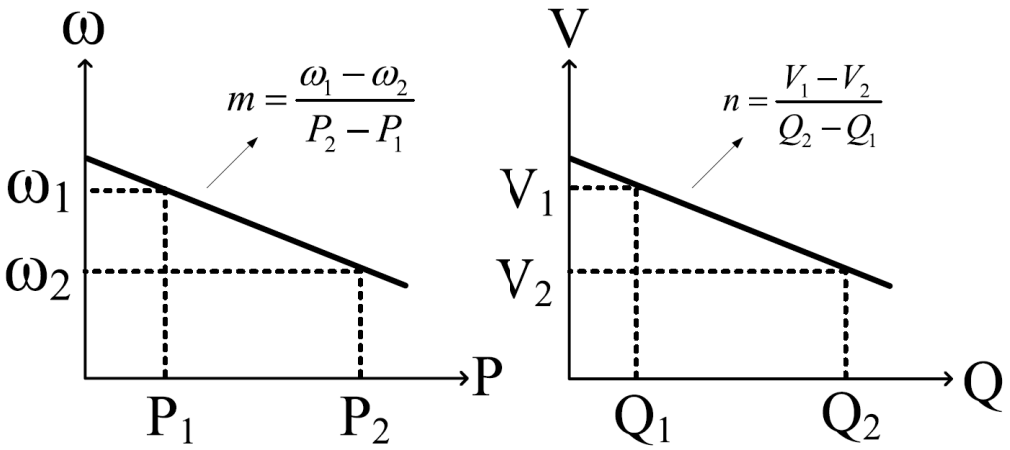

Fig. 5. Droop characteristic curves.

Mathematical Model of Microgrid

e) Voltage Controllers: The reference frequency and voltage magnitude generated by the droop equations are used as set point values for the voltage controllers. Standard PI controllers are used for this purpose, as shown in Fig. 6. The process variables are the angular frequency ω from the PLL and the measured q-axis voltage (v_{oq})

$$\dot{\varphi}_d = \omega_{PLL} - \omega^*, \tag{8a}$$
$$i_{ld}^* = k_{iv,d}\varphi_d + K_{pv,d}\dot{\varphi}_d, \tag{8b}$$
$$\dot{\varphi}_q = v_{oq}^* - v_{oq}, \tag{8c}$$
$$i_{lq}^* = k_{iv,q}\varphi_q + k_{pv,q}\dot{\varphi}_q. \tag{8d}$$

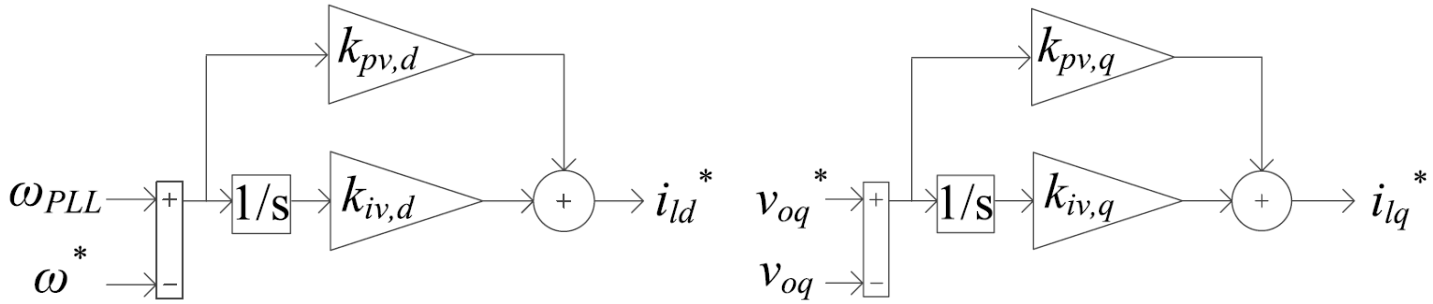

Fig. 6. The diagram of voltage controllers.

Mathematical Model of Microgrid

f) Current Controllers: Another set of PI controllers are used for current controllers as shown in Fig.7. These controllers take the difference between the commanded filter inductor currents (i^*_{ldq}), the measured filter inductor currents (i_{ldq}), and produce commanded voltage values (v^*_{ldq}). The values of correspond to the inverter output voltages before the LCL filter. Cross-coupling component terms are eliminated in these controllers as well

$$\dot{\gamma}_d = i^*_{ld} - i_{ld}, \tag{9a}$$

$$v^*_{ld} = -\omega_n L_f i_{lq} + k_{ic,d}\gamma_d + k_{pc,d}\dot{\gamma}_d, \tag{9b}$$

$$\dot{\gamma}_q = i^*_{lq} - i_{lq}, \tag{9c}$$

$$v^*_{lq} = -\omega_n L_f i_{ld} + k_{ic,q}\gamma_q + k_{pc,q}\dot{\gamma}_q. \tag{9d}$$

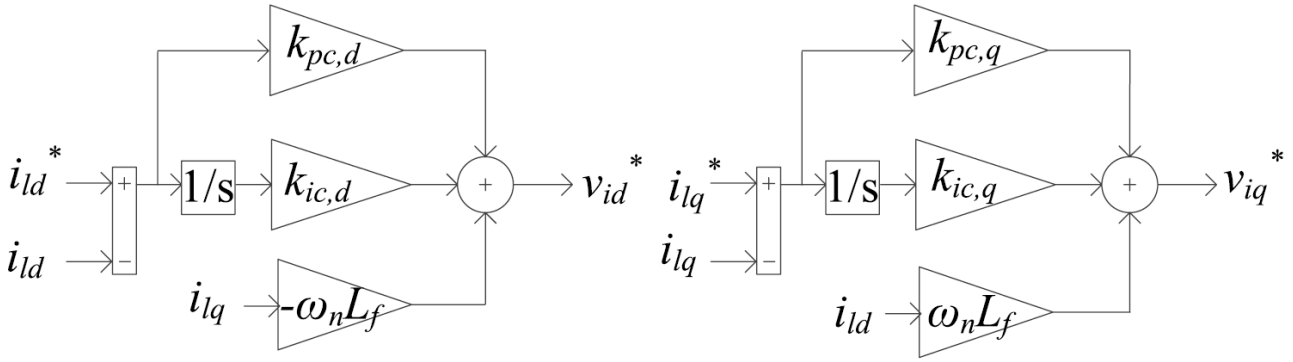

Fig. 7. The diagram of current controllers.

Mathematical Model of Microgrid

g) LC Filters and Coupling Inductors: The filter in DER is shown in Fig. 8. Without any major inaccuracies, we can assume that the commanded voltage (v^*_{idq}) appears at the input of the filter inductor, i.e., $v^*_{idq} = v_{idq}$. This approach neglects only the losses in the IGBT and diodes. The state equations governing the filter dynamics are presented,

$$\dot{i}_{ld} = (-r_f i_{ld} + v_{ld} - v_{od})/L_f + \omega_n i_{lq}, \quad (10a)$$

$$\dot{i}_{lq} = (-r_f i_{lq} + v_{lq} - v_{oq})/L_f - \omega_n i_{ld}, \quad (10b)$$

$$\dot{i}_{od} = (-r_c i_{od} + v_{od} - v_{bd})/L_c + \omega_n i_{oq}, \quad (10c)$$

$$\dot{i}_{oq} = (-r_c i_{oq} + v_{oq} - v_{bq})/L_c - \omega_n i_{od}, \quad (10d)$$

$$\dot{v}_{od} = (i_{ld} - i_{od})/C_f + \omega_n v_{oq} + R_d(\dot{i}_{ld} - \dot{i}_{od}), \quad (10e)$$

$$\dot{v}_{oq} = (i_{lq} - i_{oq})/C_f - \omega_n v_{od} + R_d(\dot{i}_{lq} - \dot{i}_{oq}). \quad (10f)$$

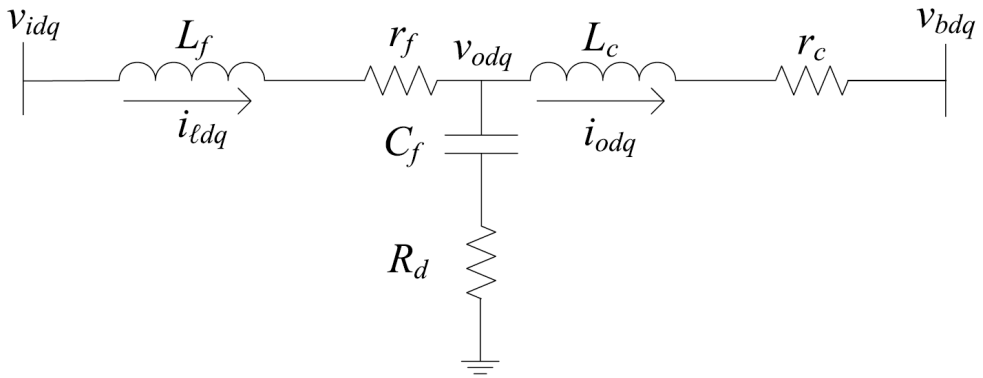

Fig. 8. The diagram of LCL filters.

Mathematical Model of Microgrid

h) Load models: The loads for this system are chosen as combination of resistors and inductors (RL loads). A typical RL load connected to an inverter bus is shown in Fig. 9. Line 'a' connected to the bus represents the base load and line 'b' works as a variable load for that bus. To check the system's dynamic behavior, a load perturbation is done on 'b'. Line 'b' appears in parallel to 'a' when the breaker closes the contact. State equations describing the load dynamics are,

$$\dot{i}_{loadD} = (-R_{load} i_{loadD} + v_{bD})/L_{load} + \omega_{PLL} i_{loadQ}, \quad (11a)$$

$$\dot{i}_{loadQ} = (-R_{load} i_{loadQ} + v_{bQ})/L_{load} - \omega_{PLL} i_{loadD}, \quad (11b)$$

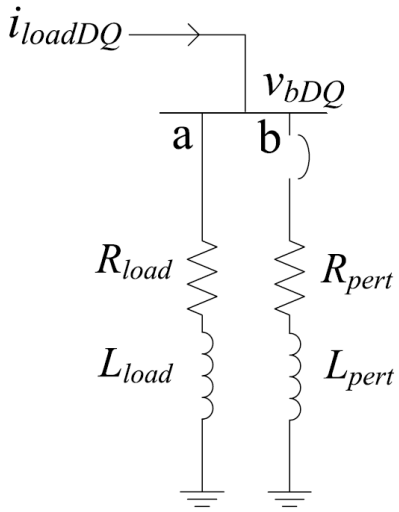

Fig. 9. Load configuration.

Mathematical Model of Microgrid

i) Distribution line: Similar to loads, the distribution line parameters consist of resistance and inductance. In Fig. 10, resistor r_{line} represents the copper loss component of the line. Inductor L_{line} is considered as the lumped inductance resulting from long line cables. Assuming that the line is connected between ith and jth bus of the system, the line dynamics are represented as follows:

$$\dot{i}_{lineDij} = (-r_{line} i_{lineD} + v_{bD,i} - v_{bD,j})/L_{line} + \omega_{PLL} i_{lineQ}, \quad (12a)$$

$$\dot{i}_{lineQij} = (-r_{line} i_{lineQ} + v_{bQ,i} - v_{bQ,j})/L_{line} - \omega_{PLL} i_{lineD}, \quad (12b)$$

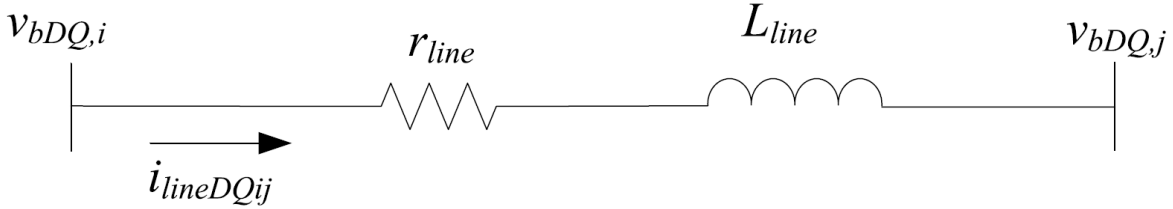

Fig. 10. Line configuration.

- The frequency is constant throughout the system.
- The variable subscript with upper case DQ denotes measurements from the global reference frame.
- First inverter's phase angle can be arbitrarily set as the reference for the entire system.

Reference Frame Transformation

Inverter bus 1 serves as the system's reference and consequently is labeled as the global reference frame. Each inverter operates in its own local reference frame. A transformation is necessary to translate between values defined in the local reference frame to the global reference frame. An application of this transformation is shown graphically in Fig. 11.

$$\begin{bmatrix} f_D \\ f_Q \end{bmatrix}_{global} = \begin{bmatrix} \cos\theta & \sin\theta \\ -\sin\theta & \cos\theta \end{bmatrix} \begin{bmatrix} f_D \\ f_Q \end{bmatrix}_{local}, \quad (13a)$$

$$\begin{bmatrix} f_D \\ f_Q \end{bmatrix}_{local} = \begin{bmatrix} \cos\theta & \sin\theta \\ -\sin\theta & \cos\theta \end{bmatrix} \begin{bmatrix} f_D \\ f_Q \end{bmatrix}_{global}, \quad (13b)$$

where θ is the difference between the global reference phase and the local reference phase, as shown in Fig. 12.

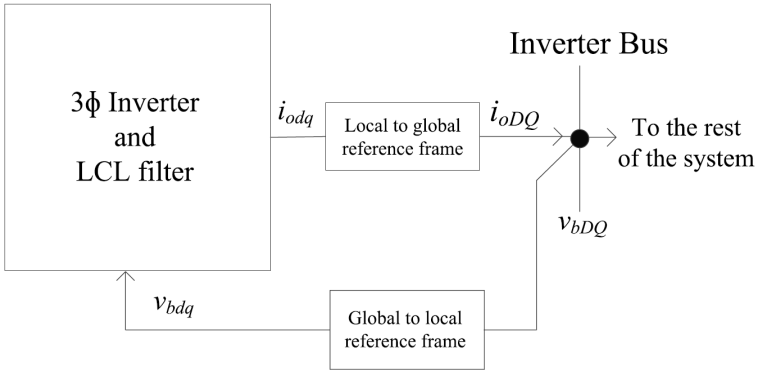

Fig. 11. Reference frame transformation.

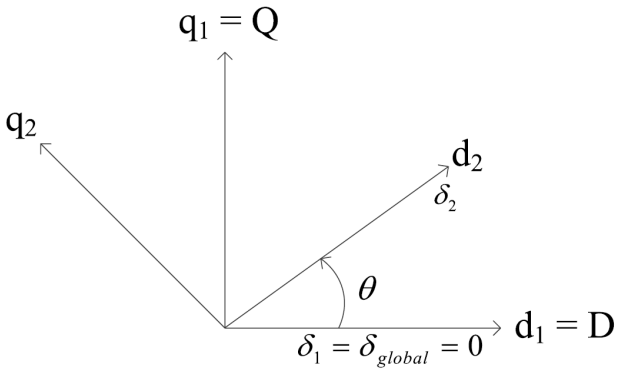

Fig. 12. Transformation angle.

State Space Model of Microgrid

The mathematical model of microgrid has been established as equation (1)-(13). We can represent this model in general state space equations as follows,

$$\dot{x} = f(x, u). \tag{14}$$

When the operation mode changes, the model structure switches as well. Therefore, we can define the state vectors in grid-tied (x_G) and islanded (x_I) modes, respectively.

$$x_G = [\delta_i, P_i, Q_i, \varphi_{Pi}, \varphi_{Qi}, \gamma_{di}, \gamma_{qi}, i_{ldi}, i_{lqi}, v_{odi}, v_{oqi}, i_{odi} \; i_{oqi}, \varphi_{PLLi}, v_{od,fi}]^T, \tag{15a}$$

$$x_I = [\delta_i, P_i, Q_i, \varphi_{di}, \varphi_{qi}, \gamma_{di}, \gamma_{qi}, i_{ldi}, i_{lqi}, v_{odi}, v_{oqi}, i_{odi} \; i_{oqi}, \varphi_{PLLi}, v_{od,fi}, i_{loadDi}, i_{loadQi}, i_{lineDij}, i_{lindQij}]^T. \tag{15b}$$

The inputs are defined as

$$u_G = [P^*, Q^*]^T. \tag{16}$$

$$u_I = [v_{bDi}, v_{bQi}, \omega^*, v_{oq}^*]^T.$$

where $i, j = 1, \ldots, m, m$ is the number of inverters in microgrid.

Bus voltages

Control signal generated by secondary control

Linearization of microgrid model

The above model is a nonlinear model. To simplify the problem, sometimes we need to obtain the small-signal model of microgrids. Let (x_e, u_e) be an equilibrium of system (14), then we can take the Taylor Series expansion of $f(x,u)$ around (x_e, u_e) as follows,

$$f(x,u) = f(x_e,u_e) + A(x-x_e) + B(u-u_e) + high\ order\ term,$$

$$A = \begin{bmatrix} \frac{\partial f_1}{\partial x_1} & \cdots & \frac{\partial f_1}{\partial x_n} \\ \vdots & \ddots & \vdots \\ \frac{\partial f_n}{\partial x_1} & \cdots & \frac{\partial f_n}{\partial x_n} \end{bmatrix}_{x=x_e}, B = \begin{bmatrix} \frac{\partial f_1}{\partial u_1} & \cdots & \frac{\partial f_1}{\partial u_{2m}} \\ \vdots & \ddots & \vdots \\ \frac{\partial f_n}{\partial u_1} & \cdots & \frac{\partial f_n}{\partial u_{2m}} \end{bmatrix}_{u=u_e}, \quad (17)$$

where n is the total order of microgrid, and m is the number of inverters in the microgrid. Define the perturbation of states and inputs as $\partial x = x - x_e$, and $\partial u = u - u_e$.

- Since (x_e, u_e) is an equilibrium, $f(x_e, u_e) = 0$.
- When the perturbation is small enough, we can neglect the high order terms.

Then we have

$$\partial \dot{x} = A\partial x + B\partial u \quad (18)$$

Virtual Resistor Method

- In the above model, bus voltages were used as an input to the system, thus, effects of load perturbation could not be accurately predicted.
- However, in practice, the only perturbation that occurs in the system comes from the step change in load. A method is needed to include the terms relating to the bus voltages in the system matrix A.
- To do this, a virtual resistor with high resistance can be assumed connected at the inverter bus. This resistor (r_n), shown in Fig. 13, has a negligible impact on system dynamics.
- Using Kirchhoff's voltage law (KVL), the equations describing the bus voltage in terms of the inverter, load currents and line currents can be expressed. This is shown in

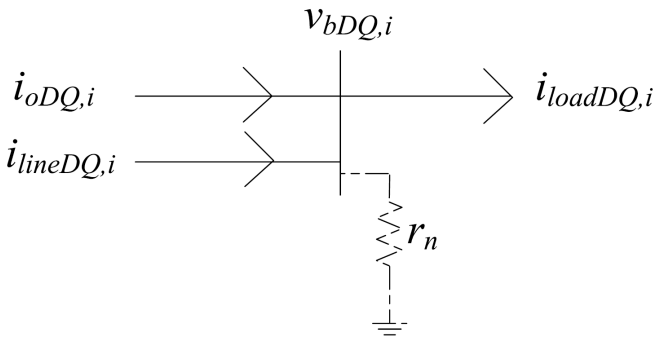

Fig. 13. Virtual resistor at a DER bus.

$$v_{bD} = r_n(i_{oD} + i_{lineD} - i_{loadD}), \quad (19a)$$

$$v_{bQ} = r_n\left(i_{oQ} + i_{lineQ} - i_{loadQ}\right). \quad (19b)$$

$$\partial\dot{x}_I = A_{sys}\partial x_I + B_{sys}\partial\tilde{u}_I \quad (20a)$$

$$\tilde{u}_I = \left[\omega^*, v_{oq}^*\right] \quad (20b)$$

Model Order Reduction Method using Singular Perturbation

- Existing microgrid models have many state variables, thus increasing the computational burden and difficulty of stability analysis.
- The dynamical model exhibits behaviors at two time-scales: faster dynamics for converters and PI controllers; and slower dynamics for power calculator and droop controller.
- The reduced-order model is developed based on the singular perturbation theory that separates the system states into fast and slow dynamics.

Consider a singular perturbation model of a dynamical system whose derivatives of some of the states are multiplied by a small positive parameter ε (perturbation coefficient) as follows

$$\dot{x} = F(x, z, u, t, \varepsilon) \tag{21}$$

$$\varepsilon \dot{z} = G(x, z, u, t, \varepsilon) \tag{22}$$

where $x \in R^N$ representing slower dynamics, $z \in R^M$ representing faster dynamics. Let ε=0, we have

$$0 = G(x, z, u, t) \tag{23}$$

If G in (23) has at least one isolated real roots

$$z = h_i(x, u, t),\ i=1,2,\ldots,k \tag{24}$$

Model Order Reduction Method using Singular Perturbation

Substitute (24) into (21), we obtain the reduced order model as follows

$$\dot{x} = F(x, h_i(x, u, t), u, t). \tag{25}$$

Note that the dimension of (1) is reduced from $n+m$ to n.

Compared to conventional order reduction that simply ignores some dynamic states, our method uses slower dynamics to represent faster ones, thus reducing order while maintaining all dynamic characteristics.

Even though we can get the reduced-order model using the above method, the accuracy of the reduced model is not guaranteed. Define a new time variable $\tau = (t - t_0)/\varepsilon$, and introduce the boundary-layer model as follows,

$$\frac{dy}{d\tau} = g(t, x, y + h(t, x), 0). \tag{26}$$

where $y=z-h(t,x)$ is the change of state variables.

Order Reduction Method for Small-Signal Microgrid Model

Then we can specify the singular perturbation theory for small-signal (linear) systems. First, we need to identify the slow and fast dynamics. For linear system, we can use the modal analysis by calculating the participation factor:

$$P_{ij} = \frac{|u_{ij}^T||v_{ij}|}{\sum_{k=1}^{N}|u_{kj}^T||v_{jk}|}, \tag{27}$$

where u_{ij} and v_{ij} are left and right eigenvectors, respectively. Using the participation factor we can know that which eigenvalue participates mostly in which state. Then based on the magnitudes of their corresponding eigenvalues, we can determine the states with larger eigenvalues as fast states, while the others as slow states. For example,

Index	Eigenvalues	Major participants	
3	−7853.98	$v_{od,f}$	fast
14, 15	−2280.14 ± j35916.37	v_{od}, v_{oq}	
12, 13	−2241.42 ± j35209.50	i_{od}, i_{oq}	
10, 11	−301.94 ± j65.61	i_{ld}, i_{lq}	
1, 2	−70.27 ± j52.26	P, Q	slow
6, 7, 8, 9	−73.08 ± j33.67	$\gamma_d, \gamma_q, \varphi_P, \varphi_Q$	
4	−6.01 ± j0.09	φ_{PLL}	
5	0	δ	

Order Reduction Method for Small-Signal Microgrid Model

The order reduction algorithm for small-signal microgrid model is given in the following steps [2]:

1. Discard $\dot{\delta}_1$ (corresponding to the reference angle) by removing the corresponding row and column.
2. Rearrange the states of the original state vector x_{sys} such that the slow states (x) are placed at the upper rows and fast states (z) are placed at the lower rows. Use a transformation matrix T_r for reordering. For example, $[x_1\ x_2\ x_3]^T$ needs to be reordered as $[x_1\ x_3\ x_2]^T$. Use the transformation matrix T_r to multiply the original vector. The new state vector and steady-state operating point vectors become $x_{new} = T_r x_{sys}$ and $X_{new} = T_r X_{sys}$, respectively,

$$T_r = \begin{bmatrix} 1 & 0 & 0 \\ 0 & 0 & 1 \\ 0 & 1 & 0 \end{bmatrix}. \tag{28}$$

3. Find the new state matrix A_{new} using T_r: $A_{new} = T_r\ A_{sys} T_r^{-1}$.

[2] M. Rasheduzzaman, J. A. Mueller, and J. W. Kimball, Rasheduzzaman. "Reduced-order small-signal model of microgrid systems." IEEE Transactions on Sustainable Energy 6.4 (2015): 1292-1305.

Order Reduction Method for Small-Signal Microgrid Model

4. Separate the new state matrix and the new states as follows:

$$\begin{bmatrix} \dot{x} \\ \dot{z} \end{bmatrix} = \begin{bmatrix} A_{11} & A_{12} \\ A_{21} & A_{22} \end{bmatrix} \begin{bmatrix} x \\ z \end{bmatrix}, \tag{29}$$

$$x_{new} = \begin{bmatrix} x \\ z \end{bmatrix}, \tag{30}$$

$$X_{new} = \begin{bmatrix} X \\ Z \end{bmatrix}. \tag{31}$$

where $A_{11} \in \mathbb{R}^{N\times N}$, $A_{12} \in \mathbb{R}^{N\times M}$, $A_{21} \in \mathbb{R}^{M\times N}$, $A_{22} \in \mathbb{R}^{M\times M}$. Also, x is the representative of the slow states and z is the representative of the fast states.

5. Perform the following iteration to find the value of L for a linear system composed of two subsystems [3]:

$$L_{i+1} = A_{22}^{-1}(A_{21} + L_i A_{11} - L_i A_{12} L_i); i = 1,2, \ldots \tag{32}$$

Start with the initial value $L_0 = A_{22}^{-1} A_{21}$ and iterate 100 times. This will ensure that the eigenvalues of the reduced-order system are as close as possible to that of the slow eigenvalues of the full-order system. For this system, 100 iterations achieved excellent accuracy with minimal computational time.

[3] P. V. Kokotovic, "A Riccati equation for block-diagonalization of ill-conditioned systems," IEEE Trans. Autom. Control, vol. 20, no. 6, pp. 812–814, Dec. 1975.

Order Reduction Method for Small-Signal Microgrid Model

6. Transform the system into the following using the slow manifold condition $z_f = z + Lx$:

$$\begin{bmatrix} \dot{x} \\ \dot{z}_f \end{bmatrix} = \begin{bmatrix} A_s & A_{12} \\ 0 & A_f \end{bmatrix} \begin{bmatrix} x \\ z_f \end{bmatrix}, \tag{33}$$

where $A_s = A_{11} - A_{12}L$; $A_f = A_{22} - LA_{12}$.

7. Perform the following iteration to find the value of M:

$$M_{i+1} = [(A_{11} - A_{12}L)M_i - M_i L A_{12}]A_{22}^{-1} + A_{12}A_{22}^{-1}; i = 1,2, \ldots$$

Start with the initial value $M_0 = A_{12}A_{22}^{-1}$ and iterate 100 times as before for L.

8. Decouple the system into slow and fast time-scale using the fast manifold condition $x_s = x + Mz_f$:

$$\begin{bmatrix} \dot{x} \\ \dot{z}_f \end{bmatrix} = \begin{bmatrix} A_s & 0 \\ 0 & A_f \end{bmatrix} \begin{bmatrix} x_s \\ z_f \end{bmatrix}. \tag{34}$$

9. The operating points corresponding to the slow states become

$$X_s = (I - ML)X - MZ. \tag{35}$$

[2] M. Rasheduzzaman, J. A. Mueller, and J. W. Kimball, Rasheduzzaman. "Reduced-order small-signal model of microgrid systems." IEEE Transactions on Sustainable Energy 6.4 (2015): 1292-1305.

Order Reduction Method for Small-Signal Microgrid Model

10. To get the corrected response x_s, add $X_{s\Delta}$ to the output of X_s, where $X_{s\Delta} = MLX + MZ$. New outputs are similar to that of the dynamics obtained from the slow states of the original system.
11. Predict the fast states using algebraic solutions

$$z_f = Lx_c + z_c$$
$$\Longrightarrow z_c = -Lx_c + z_f = -Lx_c + (LX + Z). \quad (36)$$

12. The reduced-order system is now ready for simulation. Fig. 14 shows the final arrangement for obtaining the dynamic response considering both the slow and the fast states.

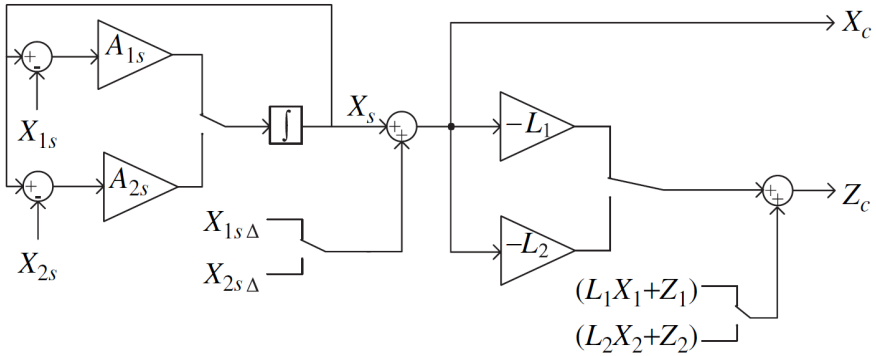

Fig. 14. Corrected response from the reduced-order model.

[2] M. Rasheduzzaman, J. A. Mueller, and J. W. Kimball, Rasheduzzaman. "Reduced-order small-signal model of microgrid systems." IEEE Transactions on Sustainable Energy 6.4 (2015): 1292-1305.

Simulation Validation of Small-Signal Order Reduction

Simulation setup: For the grid-tied system, a set of linearization points is obtained with $u = [0\ 0]^T$ to evaluate the initial higher order matrices A, B in (12) as [2]. The parameter setting is given in TABLE I. Using modal analysis we can identify the slow/fast states as follows,

$$x = [P, Q, \delta, \varphi_P, \varphi_Q, \gamma_d, \gamma_q, \varphi_{PLL}], \tag{37}$$

$$z = [i_{ld}, i_{lq}, v_{od}, v_{oq}, i_{od}\ i_{oq}, v_{od,f}]. \tag{38}$$

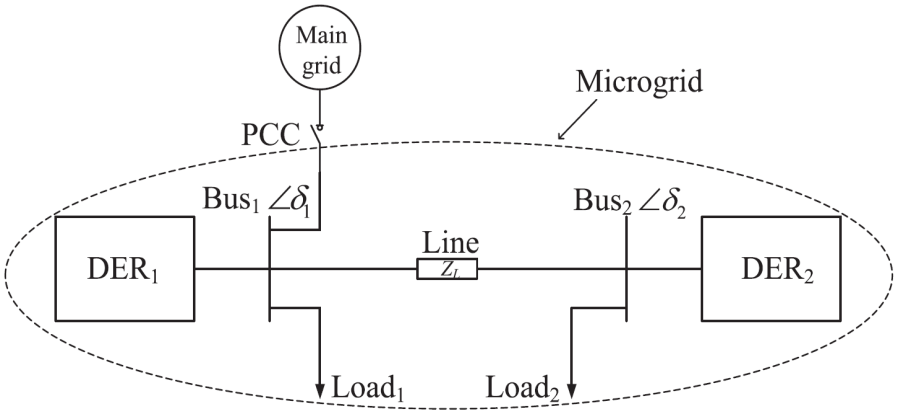

Fig. 15. Two-bus microgrid system [1].

TABLE I
PARAMETERS OF MICROGRID SYSTEM

Parameter	Value	Parameter	Value
L_f	3.90 mH	R_f	0.50 Ω
C_f	16 μf	R_d	2.05 Ω
$K_{P,P}$	0.01	$K_{I,P}$	0.10
$K_{P,C}$	1.00	$K_{I,C}$	100
$K_{P,PLL}$	0.25	$K_{I,PLL}$	2.00
ω_c	50.26 rad/s	ω_n	377 rad/s
ω_{cPLL}	7853.98 rad/s	V_{bD}	0.61 V
V_{bQ}	84.52 V		

[1] M. Rasheduzzaman, J. A. Mueller, and J. W. Kimball, "An accurate small-signal model of inverter-dominated islanded microgrids using dq reference frame," IEEE J. Emerg. Sel. Topics Power Electron., vol. 2, no. 4, pp. 1070–1080, Dec. 2014.
[2] M. Rasheduzzaman, J. A. Mueller, and J. W. Kimball, Rasheduzzaman. "Reduced-order small-signal model of microgrid systems." IEEE Transactions on Sustainable Energy 6.4 (2015): 1292-1305.

Simulation Validation of Small-Signal Order Reduction

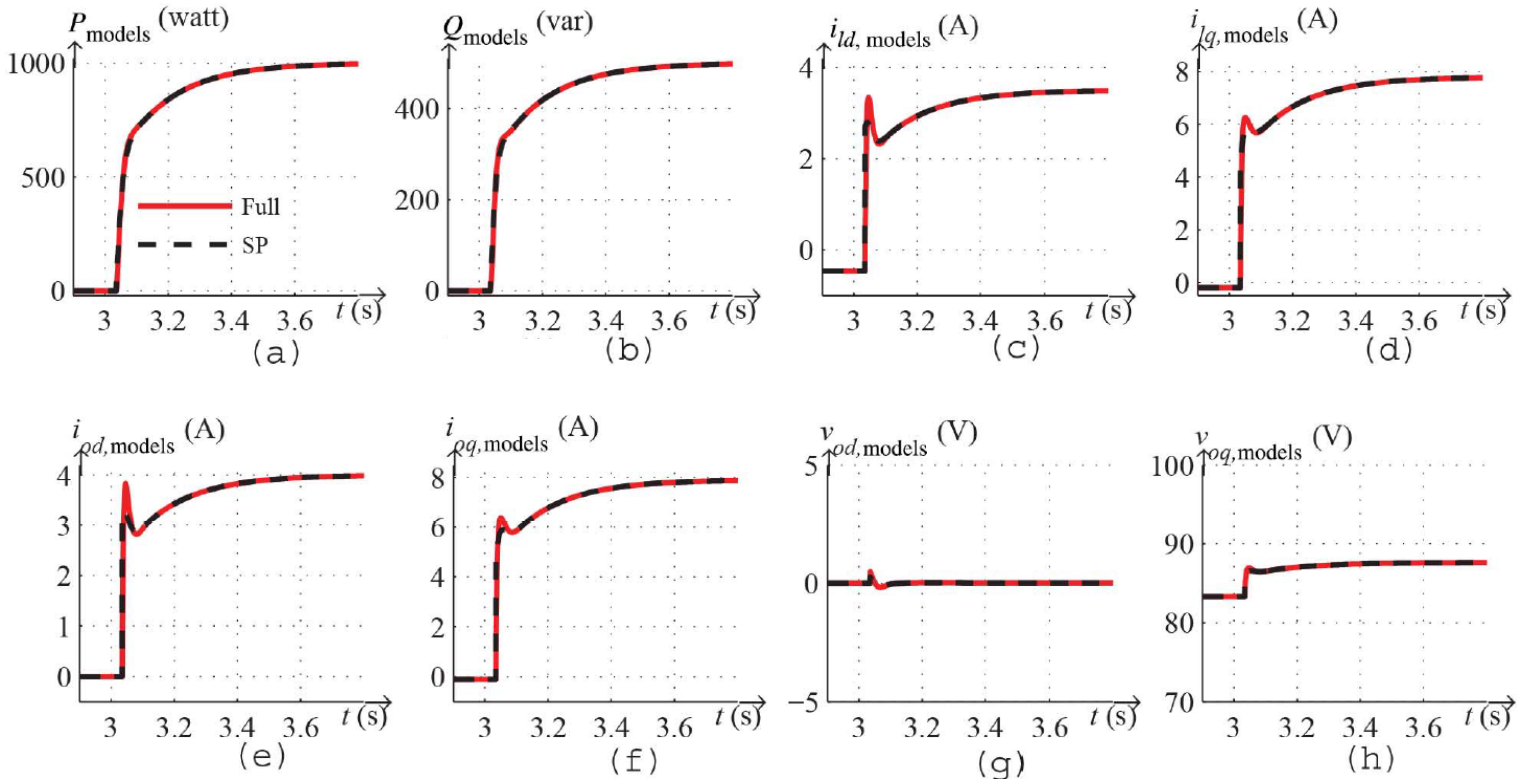

Fig. 16. Verification of the system dynamics of interests. (a) Active power. (b) Reactive power. (c) d-axis inductor current. (d) q-axis inductor current. (e) d-axis output current. (f) q-axis output current. (g) d-axis output voltage. (h) q-axis output voltage [2].

[2] M. Rasheduzzaman, J. A. Mueller, and J. W. Kimball, Rasheduzzaman. "Reduced-order small-signal model of microgrid systems." IEEE Transactions on Sustainable Energy 6.4 (2015): 1292-1305.

Simulation Validation of Small-Signal Order Reduction

Simulation setup: For the islanded system, the equilibrium point and parameter setting is defined as [2]. The modal analysis result is shown in TABLE II.

TABLE II
EIGENVALUES OF SYSTEM MATRIX A

Index	Eigenvalues	Major participants
1,2	$-7.10\times10^{8} \pm j376.57$	$i_{\text{line}DQ}$
3,4	$-2.09\times10^{8} \pm j376.58$	i_{odq1}, i_{odq2}
5,6	$-1951.65 \pm j10980.03$	v_{oq1}, v_{oq2}
7,8	$-1781.19 \pm j10234.93$	v_{od1}, v_{od2}
9	-7981.28	$v_{od1,f}$, $v_{od2,f}$
10	-7915.62	$v_{od1,f}$, $v_{od2,f}$
11,12	$-822.46 \pm j5415.18$	v_{oq1}, v_{oq2}
13,14	$-674.16 \pm j4643.15$	v_{od1}, v_{od2}
15,16	$-2889.85 \pm j351.71$	$i_{\text{load}DQ1}$, $i_{\text{load}DQ2}$
17,18	$-1500.35 \pm j336.76$	$i_{\text{load}DQ1}$, $i_{\text{load}DQ2}$
19,20	$-267.94 \pm j82.01$	i_{ldq1}, i_{ldq2}
21,22	$-69.76 \pm j21.47$	γ_{dq1}, γ_{dq2}
27,28	$-25.38 \pm j31.18$	φ_{q1}, γ_{q1}, φ_{q2}, γ_{q2}
29,30	$-6.16 \pm j22.90$	φ_{d1}, γ_{d1}, φ_{d2}, γ_{d2}
34,35	$-2.24 \pm j4.68$	φ_{dq1}, φ_{dq2}
31,32	$-10.65 \pm j8.14$	δ_2, φ_{PLL1}, φ_{PLL2}
33	-7.53	δ_2, φ_{PLL1}, φ_{PLL2}
23,24	$-50.25 \pm j0.02$	P_1, Q_1, P_2, Q_2
25	-50.27	P_1, Q_1, P_2, Q_2
26	-50.27	P_1, Q_1, P_2, Q_2
36	0	δ_1

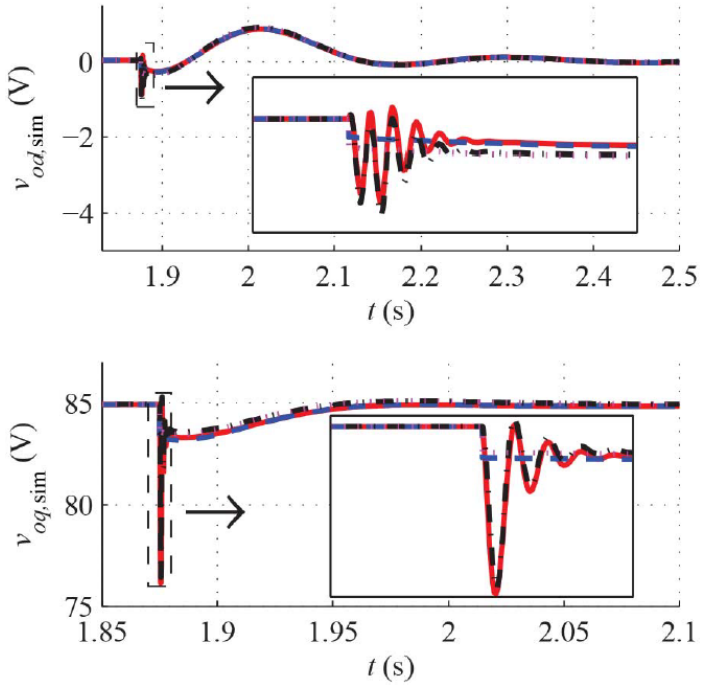

Fig. 17. Fast states marked with rectangles, are oscillatory in the full-order model but disappear in the reduced-order model and become straight lines.

[2] M. Rasheduzzaman, J. A. Mueller, and J. W. Kimball, Rasheduzzaman. "Reduced-order small-signal model of microgrid systems." IEEE Transactions on Sustainable Energy 6.4 (2015): 1292-1305.

Simulation Validation of Small-Signal Order Reduction

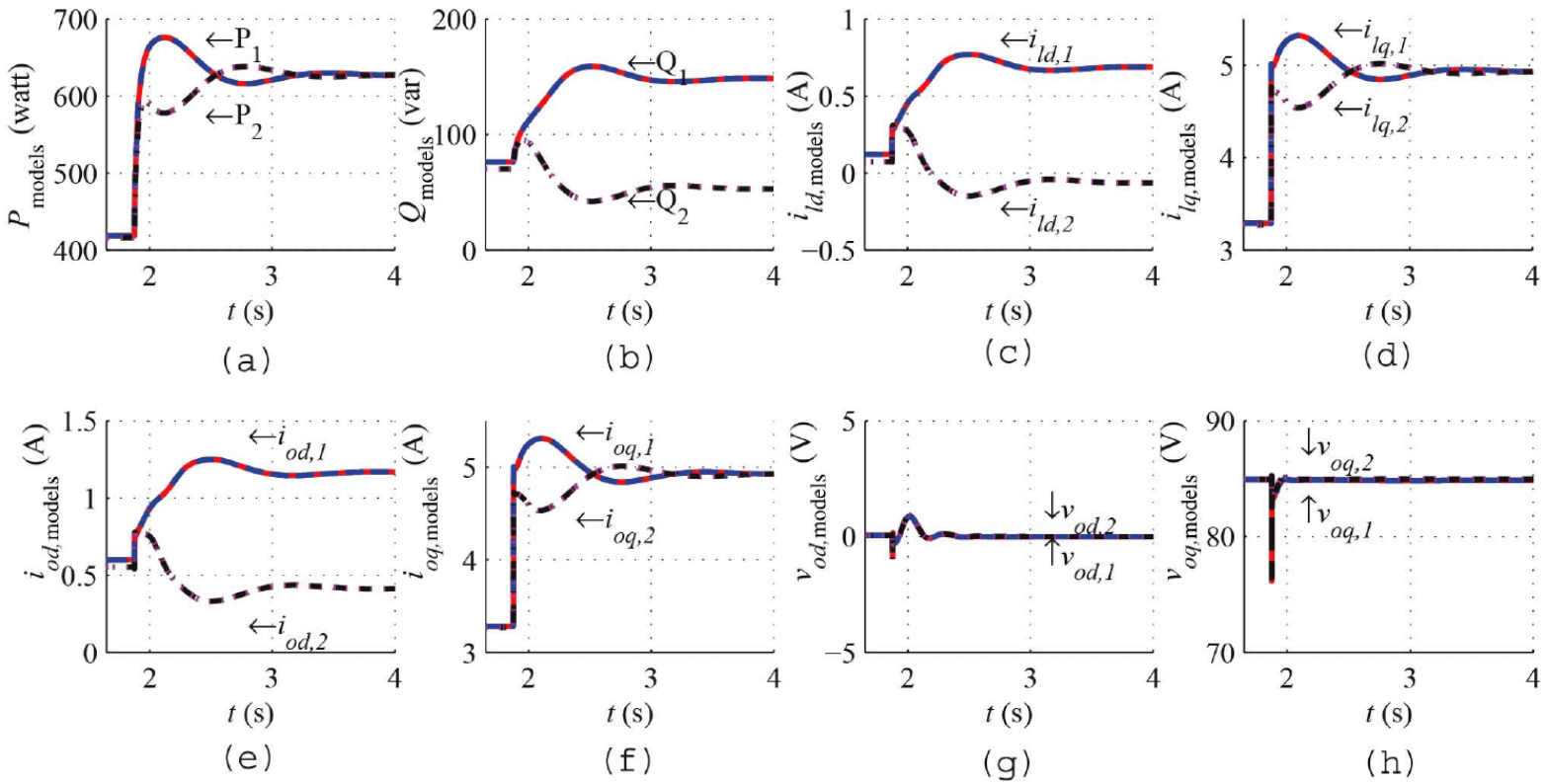

Fig. 18 Verification of system dynamics using results from experiment, full-order model simulation, and reduced-order model simulation. (a) Active power. (b) Reactive power. (c) d-axis inductor current. (d) q-axis inductor current. (e) d-axis output current. (f) q-axis output current. (g) d-axis output voltage. (h) q-axis output voltage. [2].

[2] M. Rasheduzzaman, J. A. Mueller, and J. W. Kimball, Rasheduzzaman. "Reduced-order small-signal model of microgrid systems." IEEE Transactions on Sustainable Energy 6.4 (2015): 1292-1305.

Microgrids Control: Primary and Secondary

- Microgrids control: Primary and Secondary
  - Primary control
    - Active Load Sharing
    - Droop Characteristic Techniques
    - Discussion of Primary Control Level Techniques
  - Secondary control
    - Literature Review of Secondary Control
    - Distributed Cooperative Secondary Control of Microgrids Using Feedback Linearization

Hierarchical Control of Microgrids

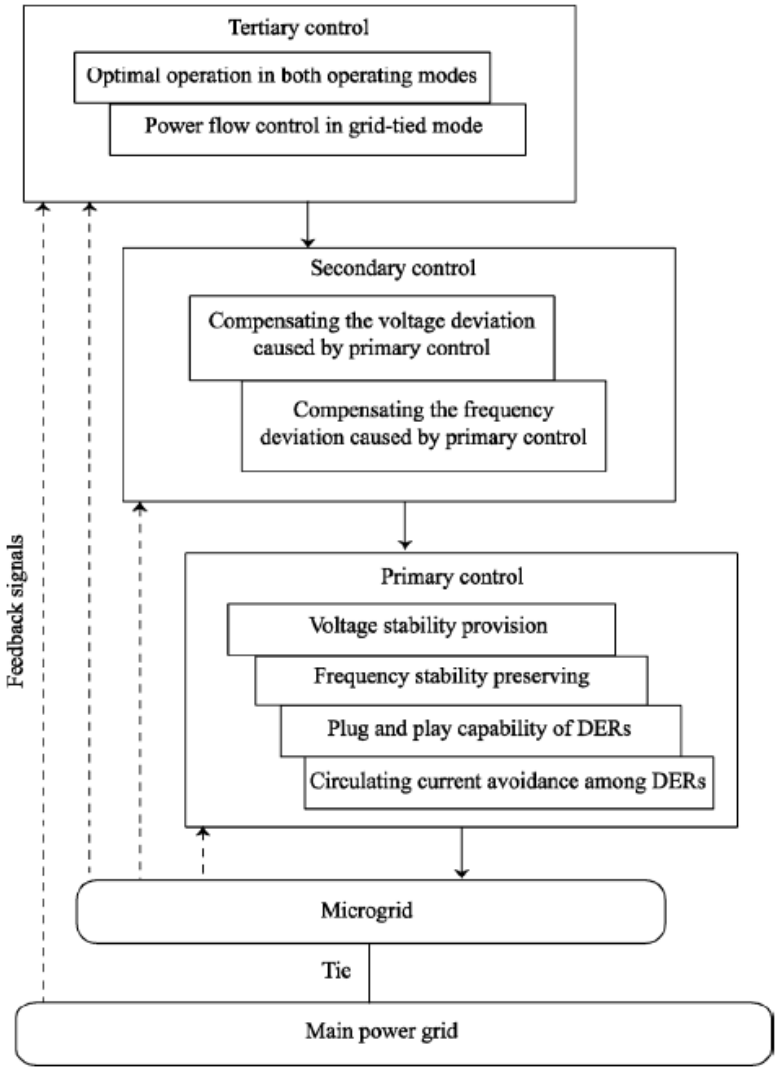

Fig. 19 Hierarchical control levels of a MG [4]

1. **Primary control**
   - To stabilize the voltage and frequency. Subsequent to an islanding event, the MG may lose its voltage and frequency stability due to the mismatch between the power generated and consumed.
   - To offer plug and play capability for DERs and properly share the active and reactive power among them, preferably, without any communication links.
   - To provide the reference points for the control loops of DERs.
2. **Secondary control**
   - As a centralized controller, secondary control restores the MG voltage and frequency and compensate for the deviations caused by the primary control.
   - Secondary control is designed to have slower dynamics response than that of the primary.

[4] A. Bidram and A. Davoudi, "Hierarchical Structure of Microgrids Control System," in *IEEE Transactions on Smart Grid*, vol. 3, no. 4, pp. 1963-1976, Dec. 2012.

Hierarchical Control of Microgrids

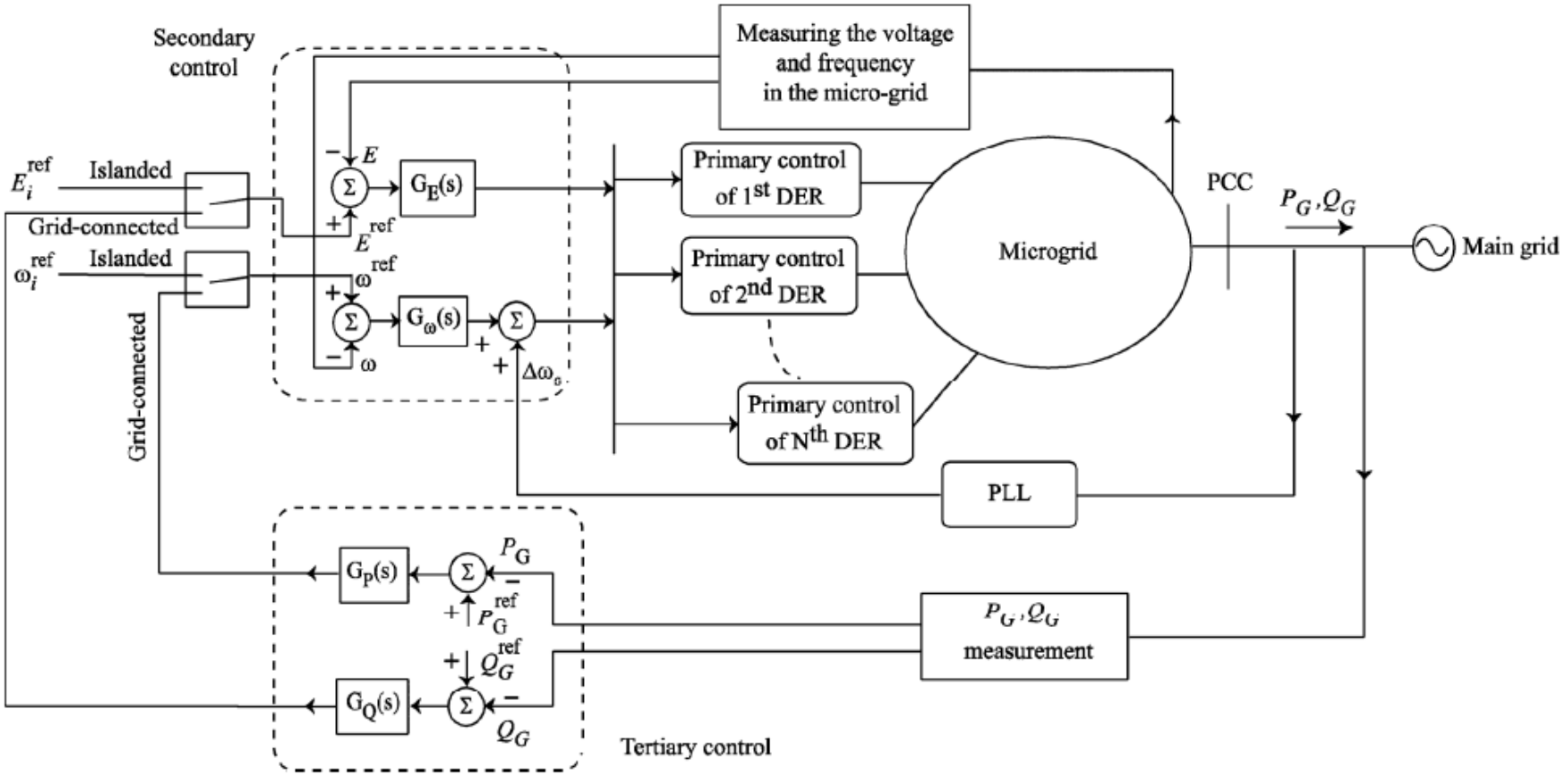

Fig. 20 Hierarchical control levels of a microgrid [4].

[4] A. Bidram and A. Davoudi, "Hierarchical Structure of Microgrids Control System," in *IEEE Transactions on Smart Grid*, vol. 3, no. 4, pp. 1963-1976, Dec. 2012.

Primary control

The primary control is designed to satisfy the following requirements:

- To stabilize the voltage and frequency. Subsequent to an islanding event, the microgrid may lose its voltage and frequency stability due to the mismatch between the power generated and consumed.
- To offer plug and play capability for DERs and properly share the active and reactive power among them, preferably, without any communication links.
- To mitigate circulating currents that can cause over-current phenomenon in the power electronic devices and damage the DC-link capacitor.

The primary control provides the reference points for the voltage and current control loops of DERs. These inner control loops are commonly referred to as zero-level control. The zero-level control is generally implemented in either PQ or voltage control modes

Primary Control: PQ Control Mode

- The control strategy is implemented with a current-controlled voltage source converter (VSC).
- H_1 controller regulates the DC-link voltage and the active power through adjusting the magnitude of the output active current of the converter i_p.
- H_2 controller regulates the output reactive power by adjusting the magnitude of the output reactive current, i.e., i_q [4].

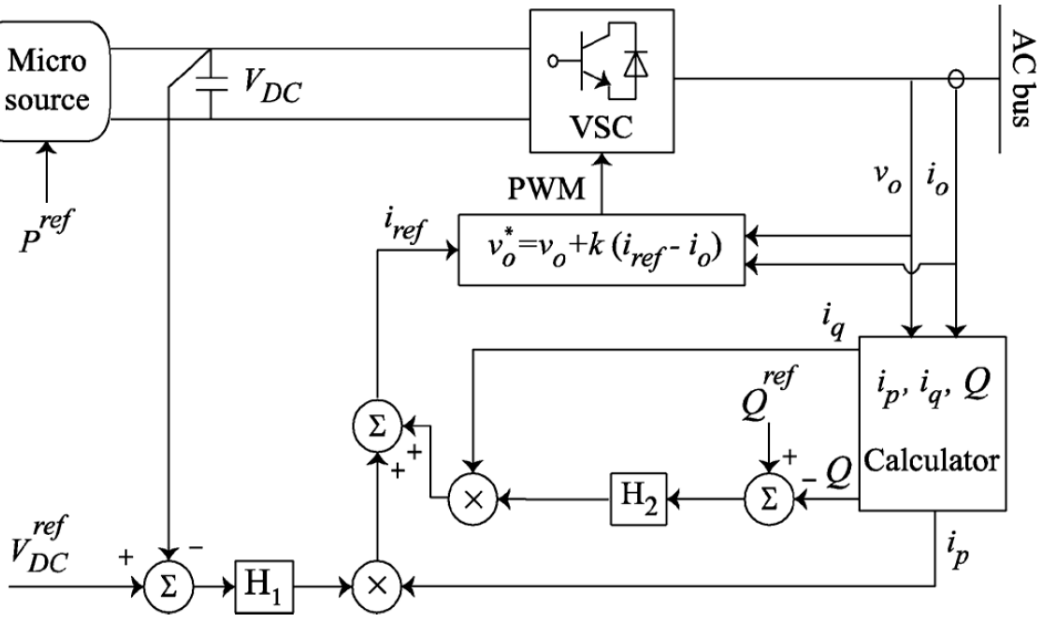

Fig. 21 PQ control mode with active and reactive power [4].

[4] A. Bidram and A. Davoudi, "Hierarchical Structure of Microgrids Control System," in *IEEE Transactions on Smart Grid*, vol. 3, no. 4, pp. 1963-1976, Dec. 2012.

Primary Control: Voltage Control Mode

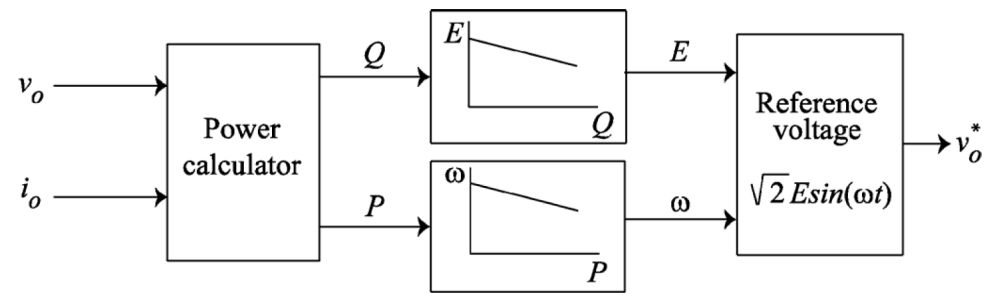

Fig. 22 Reference voltage determination for voltage control mode [4].

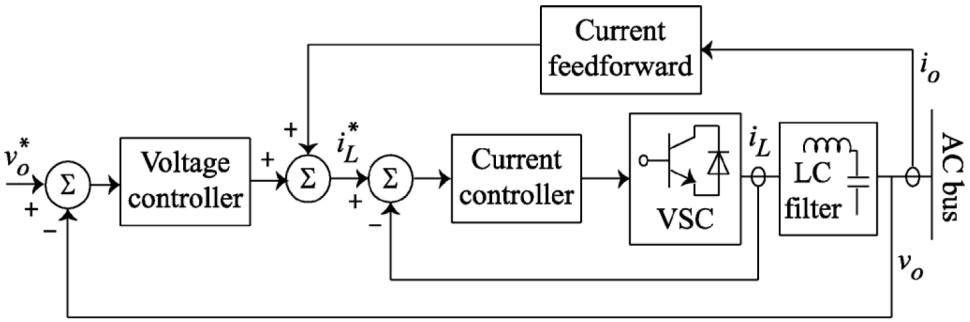

Fig. 23 Voltage and current control loops in voltage control mode [4].

- The DER operates as a voltage-controlled VSC where the reference voltage, v_0^*, is determined by the primary control, conventionally via droop characteristics, as shown in Fig. 22.
- The nested voltage and frequency control loops in the voltage control mode are shown in Fig. 23. This controller feeds the current signal as a feedforward term via a transfer function (e.g., virtual impedance).
- To fine-tune the transient response, proportional-integral-derivative (PID) [5], adaptive [6], and proportional resonant controllers [7] are proposed for the voltage controller.

[4] A. Bidram and A. Davoudi, "Hierarchical Structure of Microgrids Control System," in *IEEE Transactions on Smart Grid*, vol. 3, no. 4, pp. 1963-1976, Dec. 2012.

[5] M. J. Ryan, W. E. Brumsickle, and R. D. Lorenz, "Control topology options for single-phase UPS inverters," IEEE Trans. Ind. Appl., vol. 33, pp. 493–501, Mar./Apr. 1997.

[6] G. Escobar, P. Mattavelli, A. M. Stankovic, A. A. Valdez, and J. L. Ramos, "An adaptive control for UPS to compensate unbalance and harmonic distortion using a combined capacitor/load current sensing," IEEE Trans. Ind. Appl., vol. 54, pp. 839–847, Apr. 2007.

[7] A. Hasanzadeh, O. C. Onar, H. Mokhtari, and A. Khaligh, "A proportional-resonant controller-based wireless control strategy with a reduced number of sensors for parallel-operated UPSs," IEEE Trans. Power Del., vol. 25, pp. 468–478, Jan. 2010.

Primary Control: Zero-Level Control

- To improve the power quality for a set of energy sources connected to a common bus, the control structure shown in Fig. 24 is used.
- Each converter has an independent current control loop, and a central voltage control loop that is adopted to distribute the fundamental component of the active and reactive powers among different sources.
- The reference point for the voltage control loop is determined by the primary control.
- The individual current controllers ensure power quality by controlling the harmonic contents of the supplied currents to the common AC bus.

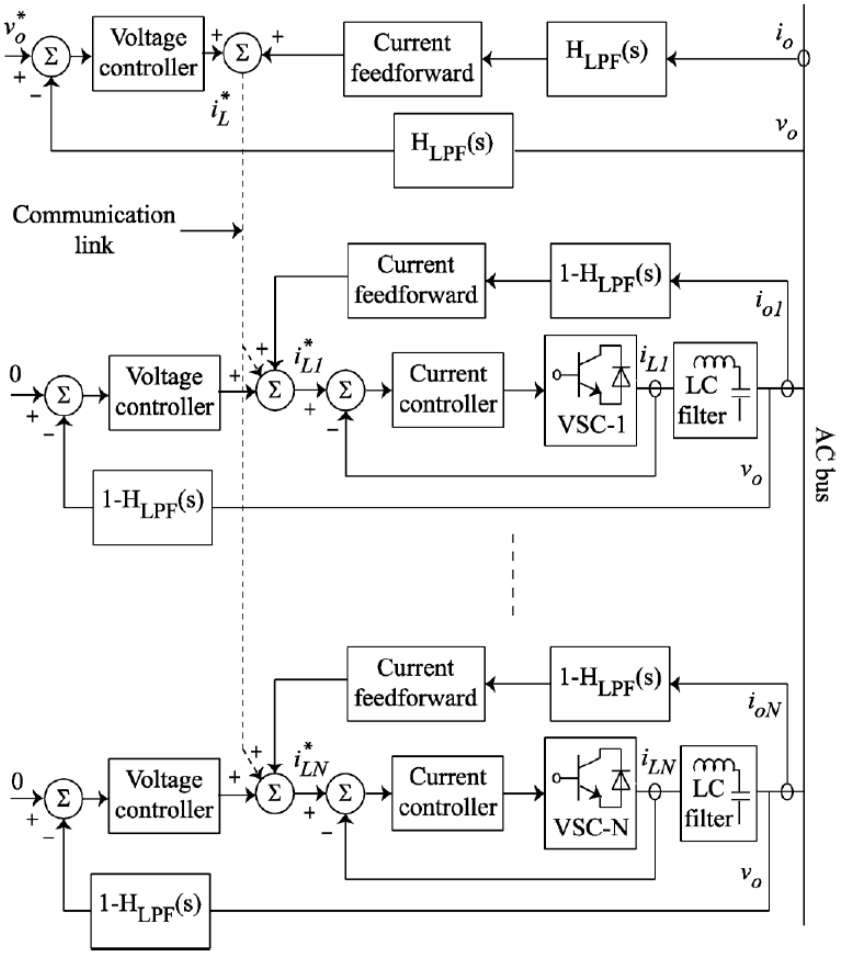

Fig. 24 Zero-level control loops for a set of energy sources connected to an AC bus [8].

[8] M. Prodanović and T. C. Green, "High-quality power generation through distributed control of a power park microgrid," IEEE Trans. Ind. Electron., vol. 53, pp. 1471–1482, Oct. 2006.

Primary Control: Active Load Sharing

- The active load sharing is a communication-based method used in parallel configuration of converters. Different approaches such as centralized, master-slave, average load sharing, and circular chain control methods [4].
  - In a centralized control method, the overall load current is evenly distributed among the sources by assigning the same current set points for all converters.
  - In the master-slave control, the master converter operates as a VSC and regulates the output voltage while the slave converters behave as individual current source converters that follow the current pattern of the master converter.
  - In the average load sharing control, the current reference for individual converters is continuously updated as the weighted average current of all converters (but not the load current).
  - In the circular chain control, converter modules are considered to be connected like links of a chain, and the current reference for each converter is determined by that of the previous converter.
- The active load sharing method requires communication links and high bandwidth control loops. However, it offers precise current sharing and high power quality.

[4] A. Bidram and A. Davoudi, "Hierarchical Structure of Microgrids Control System," in *IEEE Transactions on Smart Grid*, vol. 3, no. 4, pp. 1963-1976, Dec. 2012.

Primary Control: Droop Characteristic Techniques

The droop control method has been referred to as the independent, autonomous, and wireless control due to elimination of intercommunication links between the converters.

- The conventional active power control (frequency droop characteristic) and reactive power control (voltage droop characteristic), those illustrated in Fig. 25, are used for voltage mode control.
- Principles of the conventional droop methods can be explained by considering an equivalent circuit of a VSC connected to an AC bus, as shown in Fig. 7. If switching ripples and high frequency harmonics are neglected, the VSC can be modeled as an AC source, with the voltage of $E\angle\delta$.

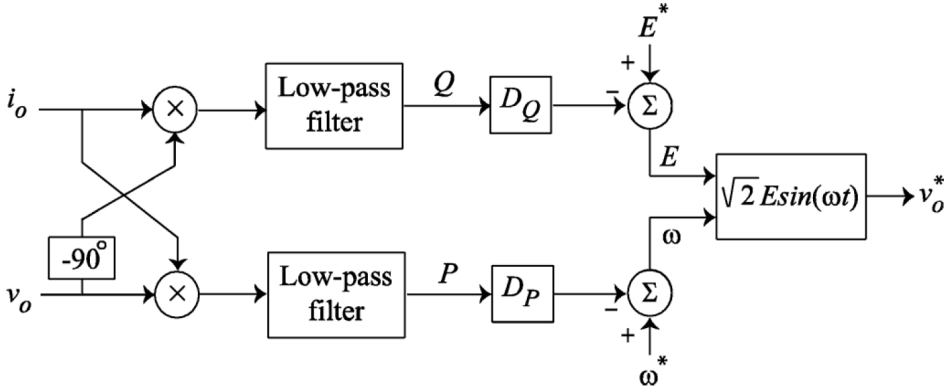

Fig. 25 Conventional droop method.

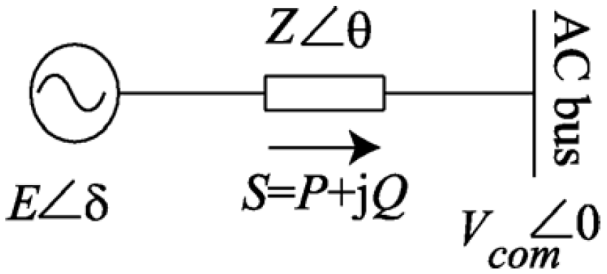

Fig. 26 Conventional droop method.

Primary Control: Droop Characteristic Techniques

In addition, assume that the common AC bus voltage is $V_{com}\angle 0$ and the converter output impedance and the line impedance are lumped as a single effective line impedance of $Z\angle\theta$. The complex power delivered to the common AC bus is calculated as

$$S = V_{com}I^* = \frac{V_{com}E\angle\theta - \delta}{Z} - \frac{V_{com}^2\angle\theta}{Z}. \tag{39}$$

from which the real and reactive powers are achieved as

$$\begin{cases} P = \frac{V_{com}E}{Z}\cos(\theta - \delta) - \frac{V_{com}^2}{Z}\cos\theta \\ Q = \frac{V_{com}E}{Z}\sin(\theta - \delta) - \frac{V_{com}^2}{Z}\sin\theta \end{cases}. \tag{40}$$

If the effective line impedance, $Z\angle\theta$, is assumed to be purely inductive, $\theta = 90°$, then (40) can be reduced to

$$\begin{cases} P = \frac{V_{com}E}{Z}\sin\delta \\ Q = \frac{V_{com}E\cos\delta - V_{com}^2}{Z} \end{cases}. \tag{41}$$

Primary Control: Droop Characteristic Techniques

If the phase difference between the converter output voltage and the common AC bus, δ, is small enough, then, $\cos\delta \approx 1$ and $\sin\delta \approx \delta$. Thus, one can apply the frequency and voltage droop characteristics to fine-tune the voltage reference of the VSC, as shown in Fig. 25 based on

$$\begin{cases} \omega = \omega^* - D_P P \\ E = E^* - D_Q Q \end{cases} \tag{42}$$

where E^* and ω^* are the DER output voltage RMS value and angular frequency at the no-load, respectively. The droop coefficients, D_P and D_Q, can be adjusted either heuristically or by tuning algorithms. In the former approach, D_P and D_Q are determined based on the converter power rating and the maximum allowable voltage and frequency deviations. For instance, in a microgrid with N DERs, corresponding D_P and D_Q should satisfy following constraints

$$\begin{cases} D_{P1}P_{n1} = D_{P2}P_{n2} = \cdots = D_{PN}P_{nN} = \Delta\omega_{max} \\ D_{Q1}Q_{n1} = D_{Q2}Q_{n2} = \cdots = D_{QN}Q_{nN} = \Delta E_{max} \end{cases} \tag{43}$$

where $\Delta\omega_{max}$ and ΔE_{max} are the maximum allowable angular frequency and voltage deviations, respectively. P_{ni} and Q_{ni} are the nominal active and reactive power of the ith DER.

Primary Control: Droop Characteristic Techniques

During the grid-tied operation of microgird, the DER voltage and angular frequency, E and ω, are enforced by the gird. The DER output active and reactive power references, P^{ref} and Q^{ref}, can hence be adjusted through E^* and ω^* as

$$\begin{cases} P^{ref} = \dfrac{\omega^* - \omega}{D_P} \\ Q^{ref} = \dfrac{E^* - E}{D_Q} \end{cases} \tag{44}$$

Dynamics response of the conventional primary control, on the simplified system of Fig. 26, can be studied by linearizing (40) and (41). For instance, the linearized active power equation in (40) and frequency droop characteristic in (41) are

$$\begin{cases} \Delta P = G\Delta\delta \\ \Delta\omega = \Delta\omega^* - D_P\Delta P \end{cases} \tag{45}$$

where at the operating point of V_{com0}, E_0 and δ_0

$$G = \frac{V_{com0}E_0}{Z}\cos\delta_0 \ \ and \ \Delta\delta = \int \Delta\omega dt. \tag{46}$$

Primary Control: Droop Characteristic Techniques

Therefore, the small-signal model for the active power control in (42) is

$$\Delta P(s) = \frac{G}{s + D_P G} \Delta\omega^*(s). \tag{47}$$

A similar procedure can be adopted to extract the small-signal model of the reactive power control. The block diagram of the small-signal model for the active power control of (42) is demonstrated in Fig. 27. As seen in (47), time constant of the closed loop control can only be adjusted by tuning D_P. On the other hand, as seen in (42), D_P also affects the DER frequency. Thus, a basic trade-off exists between the time constant of the control system and the frequency regulation.

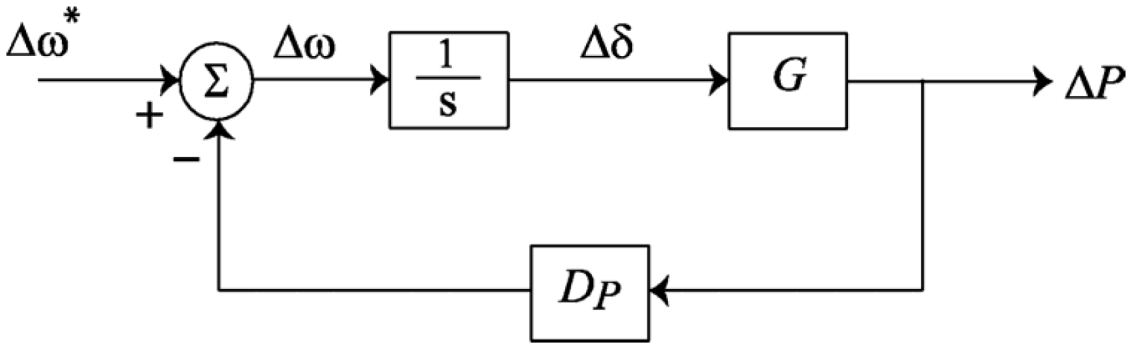

Fig. 27 Small-signal model of the conventional active power control.

Discussion of Primary Control Level Techniques

As opposed to the active load sharing technique, the conventional droop method can be implemented with no communication links, and therefore, is more reliable. However, it has some drawbacks as listed below:

- Since there is only one control variable for each droop characteristic, it is impossible to satisfy more than one control objectives. As an example, a design tradeoff needs to be considered between the time constant of the control system and the voltage and frequency regulation.
- The conventional droop method is developed assuming highly inductive effective impedance between the VSC and the AC bus. However, this assumption is challenged in microgrid applications since low-voltage transmission lines are mainly resistive. Thus, (41) is not valid for microgrid applications [4].
- As opposed to the frequency, the voltage is not a global quantity in the microgrid. Thus, the reactive power control in (42) may adversely affect the voltage regulation for critical loads [9].
- In case of nonlinear loads, the conventional droop method is unable to distinguish the load current harmonics from the circulating current. Moreover, the current harmonics distorts the DER output voltage. The conventional droop method can be modified to reduce the total harmonic distortion (THD) of the output voltages.

[4] A. Bidram and A. Davoudi, "Hierarchical Structure of Microgrids Control System," in *IEEE Transactions on Smart Grid*, vol. 3, no. 4, pp. 1963-1976, Dec. 2012.
[9] E. Rokrok and M. E. H. Golshan, “Adaptive voltage droop method for voltage source converters in an islanded multibus microgrid,” IET Gen., Trans., Dist., vol. 4, no. 5, pp. 562–578, 2010.

Discussion of Primary Control Level Techniques

TABLE III
POTENTIAL ADVANTAGES AND DISADVANTAGES OF THE DISCUSSED DROOP METHODS

Droop Method	Potential advantages	Potential disadvantages
Conventional droop method [10]	• Simple implementation	• Affected by the system parameters. • Only functional for highly inductive transmission lines. • Cannot handle nonlinear loads. • Voltage regulation is not guaranteed. • Adjusting the controller speed for the active and reactive power controllers can affect the voltage and frequency controls.
Adjustable load sharing method [11]	• Adjusting the controller speed for the active and reactive power controllers can affect the voltage and frequency controls. • Robust to the system parameter variations. • Improved voltage regulation.	• Cannot handle nonlinear loads.
VPD/FQB droop method [12]	• Simple implementation • Adjusting the controller speed for the active and reactive power controllers can affect the voltage and frequency controls.	• Affected by the system parameters. • Only functional for highly inductive transmission lines. • Cannot handle nonlinear loads.

[10] M. C. Chandorkar, D. M. Divan, and R. Adapa, "Control of parallel connected inverters in standalone AC supply systems," IEEE Trans. Ind. Appl., vol. 29, pp. 136–143, Jan./Feb. 1993.
[11] C. K. Sao and W. Lehn, "Autonomous load sharing of voltage source converters," IEEE Trans. Power Del., vol. 20, pp. 1009–1016, Apr. 2005.
[12] C. K. Sao and W. Lehn, "Control and power management of converter fed microgrids," IEEE Trans. Power Syst., vol. 23, pp. 1088–1098, Aug. 2008.

Discussion of Primary Control Level Techniques

Virtual frame transformation method [13]	• Simple implementation. • Decoupled active and reactive power controls.	• Cannot handle nonlinear loads. • The line impedances should be known a priori. • Voltage regulation is not guaranteed. • Adjusting the controller speed for the active and reactive power controllers can affect the voltage and frequency controls.
Virtual output impedance [14]	• Simple implementation. • Not affected by the system parameters. • Functional for both linear and nonlinear loads. • Mitigates the harmonic distortion of the output voltage. • Can compensate for the unbalance of the DER output voltages.	• Voltage regulation is not guaranteed. • Adjusting the controller speed for the active and reactive power controllers can affect the voltage and frequency controls.
Adaptive voltage droop method [15]	• Improved voltage regulation. • Not affected by the system parameters.	• Adjusting the controller speed for the active and reactive power controllers can affect the voltage and frequency controls. • Cannot handle nonlinear loads. • System parameters should be known a priori.
Signal injection method [16]	• Functional for both linear and nonlinear loads. • Not affected by the system parameters.	• Complicated implementation. • Voltage regulation is not guaranteed. • Adjusting the controller speed for the active and reactive power controllers can affect the voltage and frequency controls.
Nonlinear load sharing techniques [17]	• Properly shares the current harmonics between the DERs, and consequently, cancels out the voltage harmonics.	• Adjusting the controller speed for the active and reactive power controllers can affect the voltage and frequency controls. • Poor voltage regulation for the case of precise reactive power sharing. • Affected by the system parameters.

Secondary control

The primary control is designed to satisfy the following requirements:

- As a centralized controller, secondary control restores the MG voltage and frequency and compensate for the deviations caused by the primary control.
- Secondary control is designed to have slower dynamics response than that of the primary.

Primary control, as discussed, may cause frequency deviation even in steady state. Although the storage devices can compensate for this deviation, they are unable to provide the power for load-frequency control in long terms due to their short energy capacity. The secondary control, as a centralized controller, restores the microgrid voltage and frequency and compensate for the deviations caused by the primary control. This control hierarchy is designed to have slower dynamics response than that of the primary, which justifies the decoupled dynamics of the primary and the secondary control loops and facilitates their individual designs.

Differences and Connections between Primary and Secondary Control

TABLE IV
DIFFERENCES AND CONNECTIONS BETWEEN PRIMARY AND SECONDARY CONTROL

	Differences	Connections
Primary Control	• Operated in faster time-scale • Aims to stabilize the voltage and frequency • Cannot eliminate steady-state errors • Distributed local controllers	• The input reference of primary control is the control signal generated by secondary control • Since primary control has steady-state errors, the output of primary level is fed back to the secondary control as the output feedback. Then, the secondary level designs control law to realize accurate output tracking by minimizing the error between output feedback and desired values. • When designing secondary controller, the primary controlled microgrid is viewed as a plant of secondary control.
Secondary Control	• Operated in slower time-scale • Aims to restore the voltage and frequency to their reference values • Can eliminate steady-state errors • Can be centralized, decentralized or distributed.	

Conventional Secondary and Primary Control structure of Microgrids

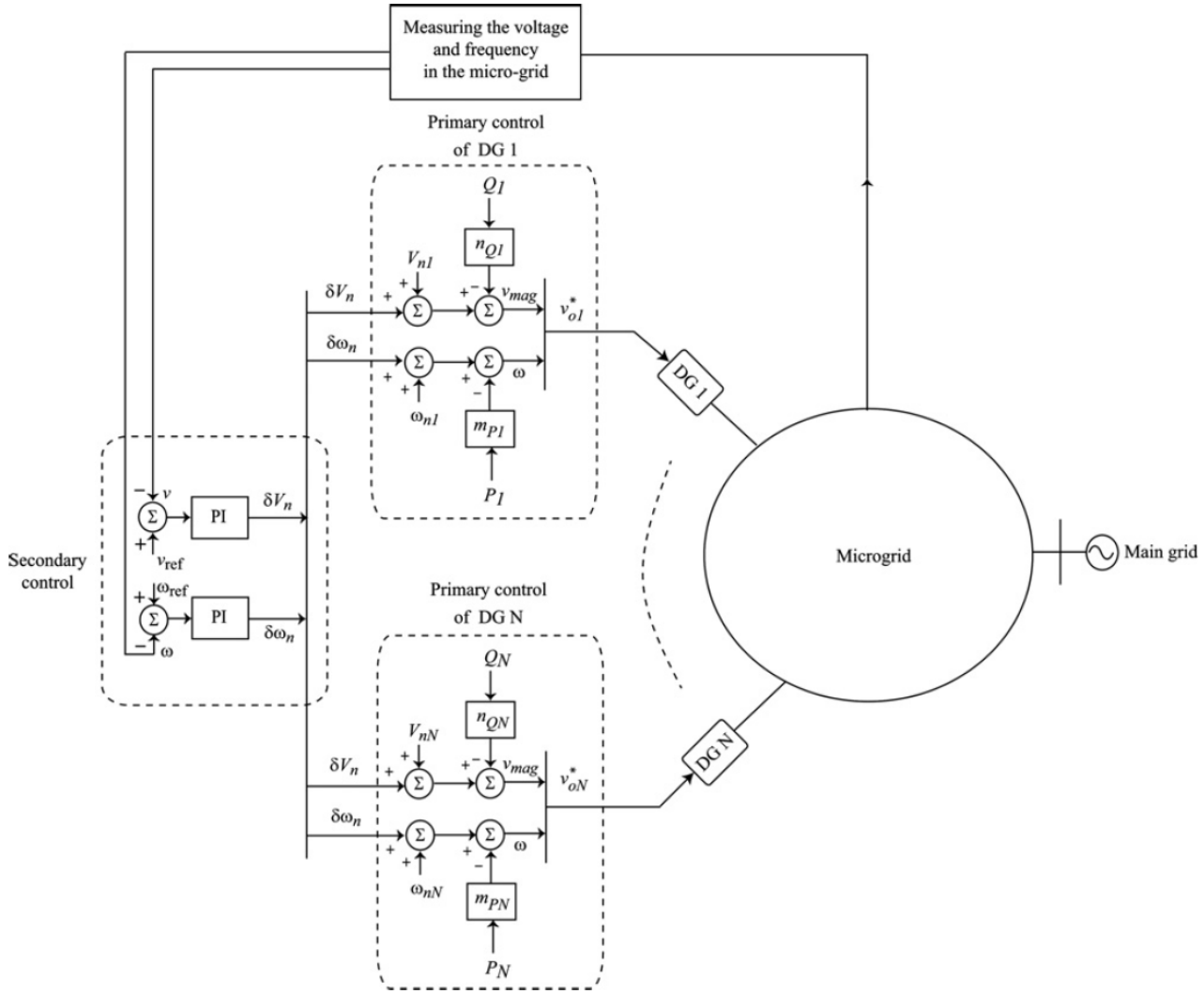

Fig. 28 Conventional control levels of a microgrid [5]

[18] A. Bidram, et al. "Secondary control of microgrids based on distributed cooperative control of multi-agent systems." IET Generation, Transmission & Distribution 7.8 (2013): 822-831.

Existing Secondary Control Methods of Microgrids

TABLE V
SECONDARY CONTROL METHODS OF MICROGRIDS

Secondary control	Centralized	• PID	• Simple implementation. • Cannot realize accurate output regulation.
		• Potential function-based optimization	• Optimal control objectives. • Requires bidirectional communication infrastructure.
		• Voltage unbalance compensation	• Satisfy the power quality requirements.
		• Feedback linearization	• Simple implementation for nonlinear systems. • Require accurate mathematical models.
	Decentralized	• Adaptive control	• Robust to the system parameter variations. • Can be extended to model-free control. • Do not need communication infrastructure.
	Distributed	• Distributed feedback linearization	• Improved reliability. • Simple implementation for nonlinear systems. • Require accurate mathematical models.
		• Distributed adaptive control	• Robust to the system parameter variations. • Can be extended to model-free control. • Improved reliability.
		• Distributed model predictive control	• Optimal control objectives. • Rolling closed-loop control. • Can deal with constraints.

Secondary Control: PID Control

When using PI controller in secondary control, frequency of the microgrid and the terminal voltage of a given DER are compared with the corresponding reference values, ω^{ref} and E^{ref}, respectively. Then, the error signals are processed by individual controllers as in (48); the resulting signals ($\delta\omega$ and δE) are sent to the primary controller of the DER to compensate for the frequency and voltage deviations

$$\begin{cases} \delta\omega = K_{P\omega}\left(\omega^{ref} - \omega\right) + K_{I\omega}\int\left(\omega^{ref} - \omega\right)dt + \Delta\omega_s \\ \delta E = K_{PE}\left(E^{ref} - E\right) + K_{IE}\int\left(E^{ref} - E\right)dt \end{cases} \tag{48}$$

where $K_{P\omega}, K_{I\omega}, K_{PE}$ and K_{IE} are the controllers parameters. An additional term, $\Delta\omega_s$, is considered in frequency controller in (48) to facilitate synchronization of the microgird to the main gird. In the islanded operating mode, this additional term is zero. However, during the synchronization, a PLL module is required to measure $\Delta\omega_s$. During the grid-tied operation, voltage and frequency of the main grid are considered as the references in (48).

Secondary Control: Potential function-based Control

Most recently, potential function-based optimization technique has been suggested for the secondary control [19]. In this method, a potential function is considered for each DER. The block diagram of the potential function-based technique is shown in Fig. 29. In this technique, when the potential functions approach their minimum values, the microgrid is about to operate at the desired states. Therefore, inside the optimizer in Fig. 29, set points of the DER are determined such that to minimize the potential functions, and thus, to meet the microgrid control objectives.

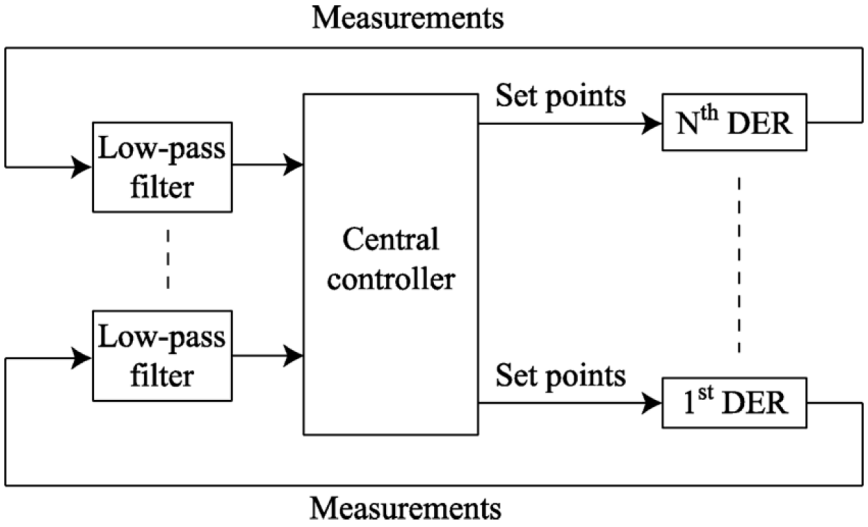

Fig. 29 The potential function-based technique block diagram [19].

[19] F. Katiraei, M. R. Iravani, and P. W. Lehn, "Microgrid autonomous operation during and subsequent to islanding process," IEEE Trans. Power Del., vol. 20, pp. 248–257, Jan. 2005.

Secondary Control: Potential function-based Control

In this method, a potential function is considered for each DER [19]. This function is a scalar cost function that carries all the information on the DER measurements, constraints, and control objectives as

$$\phi_j(x_j) = \omega^u \sum_{i=1}^{n_u} p_i^u(x_j) + \omega^c \sum_{i=1}^{n_c} p_i^c(x_j) + \omega^g p_j^g(x_j), \qquad (49)$$

where ϕ_j is the potential function related to each DER, and x_j comprises the measurements from the DER unit (e.g., voltage, current, real and reactive power). p_i^u denotes the partial potential functions that reflect the measurement information of the DER. p_i^c denotes the operation constraints that ensure the stable operation of microgrid. p_j^g is used to mitigate the DER measurements from the pre-defined set points. $\omega^u, \omega^c \; and \; \omega^g$ are the weighted factors for the partial potential functions.

[19] F. Katiraei, M. R. Iravani, and P. W. Lehn, "Microgrid autonomous operation during and subsequent to islanding process," IEEE Trans. Power Del., vol. 20, pp. 248–257, Jan. 2005.

Distributed Secondary Control: Graph Theory

- The communication network of a multiagent cooperative system can be modeled by a directed graph (digraph). A digraph is expressed as $G_r = (V_G, E_G, A_G)$ with a nonempty finite set of N nodes $V_G = (V_1, V_2, \dots, V_N)$, a set of edges or arcs $E_G \subset V_G \times V_G$, and the associated adjacency matrix $A_G = [a_{ij}] \in \mathbb{R}^{N \times N}$. In a microgrid, DGs are the nodes of the communication digraph. The edges of the corresponding digraph of the communication network represent the communication links [20].
- An edge from node j to node i is denoted by (V_j, V_i), which means that node i receives the information from node j. a_{ij} is the weight of edge (V_j, V_i) and $a_{ij} > 0$ if $(V_j, V_i) \in E_G$, otherwise $a_{ij} = 0$. Node i is called a neighbor of node j if $(V_i, V_j) \in E_G$. The set of neighbors of node j is denoted as $N_j = \{i | (V_i, V_j) \in E_G\}$. For a digraph, if node i is a neighbor of node j, then node j can get information from node i but not necessarily vice versa. The in-degree matrix is defined as $D = diag\{d_i\} \in \mathbb{R}^{N \times N}$ with $d_i = \sum_{j \in N_j} a_{ij}$. The Laplacian matrix is defined as $L = D - A_G$. A directed path from node i to node j is a sequence of edges, expressed as $\{(V_i, V_k), (V_k, V_l), \dots, (V_m, V_j)\}$.
- A digraph is said to have a spanning tree if there is a root node with a directed path from that node to every other node in the graph. A digraph is strongly connected if there is a directed path between any two nodes in the graph.

[20] A. Bidram, F. L. Lewis and A. Davoudi, "Distributed Control Systems for Small-Scale Power Networks: Using Multiagent Cooperative Control Theory," in IEEE Control Systems Magazine, vol. 34, no. 6, pp. 56-77, Dec. 2014.

Distributed Secondary Voltage Control: Feedback linearization

Recall the large-signal dynamic model of microgrid, we can rewrite it in the following control-affine form:

$$\begin{cases} \dot{x}_i = f_i(x_i) + k_i(x_i)D_i + g_i(x_i)u_i, \\ y_i = h_i(x_i), \end{cases} \tag{50}$$

where $x_i = [\delta_i, P_i, Q_i, \varphi_{Pi}, \varphi_{Qi}, \gamma_{di}, \gamma_{qi}, i_{ldi}, i_{lqi}, v_{odi}, v_{oqi}, i_{odi}, i_{oqi}, \varphi_{PLLi}, v_{od,fi}]^T$, $D_i = [\omega_{com}\ v_{bdi}\ v_{bqi}]^T$, $y_i = v_{odi}$, $u_i = E_i^*$, $f_i(x_i), k_i(x_i)\ and\ g_i(x_i)$ can be extracted from (1)-(13).

Input–output feedback linearization can be used to facilitate the secondary voltage control design. In input–output feedback linearization, a direct relationship between the dynamics of the output y_i and the control input u_i is generated by repetitively differentiating y_i with respect to time.

For the dynamics of the ith DG in (50), the direct relationship between the y_i and u_i is generated after the second derivative of the output y_i,

$$\ddot{y}_i = L_{F_i}^2 h_i + L_{g_i} L_F h_i u_i, \tag{51}$$

where

$$F_i(x_i) = f_i(x_i) + k_i(x_i)D_i. \tag{52}$$

Distributed Secondary Voltage Control: Feedback linearization

The *Lie derivative* $L_F h_i$ with respect to F_i is defined as

$$L_F h_i = \nabla h_i F_i = \frac{\partial h_i}{\partial x_i} F_i, \tag{53}$$

$$L_{F_i}^2 h_i = L_F(L_F h_i) = \frac{\partial (L_F h_i)}{\partial x_i} F_i. \tag{54}$$

An auxiliary control v_i is defined as

$$v_i = L_{F_i}^2 h_i + L_{g_i} L_F h_i u_i, \tag{55}$$

Equations (51) and (55) result in the second-order linear system

$$\ddot{y}_i = v_i, \qquad \forall\, i. \tag{56}$$

By choosing appropriate v_i, the synchronization for y_i is provided. The control input u_i is implemented by v_i as

$$u_i = \left(L_{g_i} L_F h_i\right)^{-1} \left(v_i - L_{F_i}^2 h_i\right). \tag{57}$$

To design v_i, first (56) and the first derivative of y_i are written as

$$\begin{cases} \dot{y}_i \equiv z_i, \forall\, i \\ \dot{z}_i = v_i, \forall\, i \end{cases} \tag{58}$$

where z_i is defined as the first derivative of y_i.

Distributed Secondary Voltage Control: Feedback linearization

The compact form of (58) can be written as

$$\dot{\boldsymbol{y}}_i = A\boldsymbol{y}_i + Bv_i, \forall\, i. \tag{59}$$

where $\boldsymbol{y}_i = [y_i, z_i]^T, B = [0, 1]^T$, and $A = \begin{bmatrix} 0 & 1 \\ 0 & 0 \end{bmatrix}$.

The commensurate reformulated dynamics of the reference can be expressed as

$$\dot{\boldsymbol{y}}_0 = A\boldsymbol{y}_0, \tag{60}$$

where $\boldsymbol{y}_0 = [y_0, \dot{y}_0]^T$. Since $y_0 = v_{ref}$ is constant, $\dot{y}_0 = 0$.

It is assumed that DGs can communicate with each other through a communication network described by the digraph G_r. Based on the digraph G_r, the ith DG may need to transmit $\boldsymbol{y}_i$ in (59) through the communication network. It is assumed that only one DG has access to the reference $\boldsymbol{y}_0$ in (60) by a weight factor known as the pinning gain b_i . The secondary voltage control problem is to find a distributed v_i in (57) such that DG output voltage magnitudes and their first derivatives synchronize to $\boldsymbol{y}_0$ in (60), that is, $\boldsymbol{y}_i$ synchronizes $\boldsymbol{y}_0$ for all i.

Distributed Secondary Voltage Control: Feedback linearization

To solve this problem, the cooperative team objectives are expressed in terms of the local neighborhood tracking error

$$\boldsymbol{e}_i = \sum_{j \in N_i} a_{ij}(\boldsymbol{y}_i - \boldsymbol{y}_j) + b_i(\boldsymbol{y}_i - \boldsymbol{y}_0), \tag{61}$$

where N_i denotes the set of DGs neighboring the ith DG, and a_{ij} denotes the elements of the communication digraph adjacency matrix. The pinning gain b_i is nonzero for only one DG. For a microgrid including N DGs, the global error vector for graph G_r is written from (61) as

$$\boldsymbol{e} = [(L + B) \otimes I_2](Y - Y_0) \equiv [(L + B) \otimes I_2]\boldsymbol{\delta}, \tag{62}$$

where $Y = [\boldsymbol{y}_1^T, \boldsymbol{y}_2^T, \dots, \boldsymbol{y}_N^T]^T$, $\boldsymbol{e} = [\boldsymbol{e}_1^T, \boldsymbol{e}_2^T, \dots, \boldsymbol{e}_N^T]^T$, $Y_0 = \mathbf{1}_N \boldsymbol{y}_0$ ($\mathbf{1}_N$ is the vector of ones with the length of N), $B = diag\{b_i\}$, I_2 is the 2×2 identity matrix, $\boldsymbol{\delta}$ is the global disagreement vector, $\otimes$ denotes the Kronecker product, then it follows that

$$\dot{Y} = (I_N \otimes A)Y + (I_N \otimes B)\boldsymbol{v}, \tag{63}$$

where $\boldsymbol{v} = [v_1, v_2, \dots, v_N]^{\boldsymbol{T}}$ is the global auxiliary control vector, and $\dot{Y}_0$ can be written as

$$\dot{Y}_0 = (I_N \otimes A)Y_0. \tag{64}$$

Distributed Secondary Voltage Control: Feedback linearization

Let the digraph G_r have a spanning tree and $b_i \neq 0$ for one DG placed on a root node of the digraph Gr. It is assumed that the internal dynamics of each DG are asymptotically stable. Let the auxiliary control v_i in (57) be

$$v_i = -cK\boldsymbol{e}_i, \tag{65}$$

where $c \in \mathbb{R}$ is the coupling gain and $c \in \mathbb{R}^{1\times 2}$ is the feedback control vector. Then, all $\boldsymbol{y}_i$ in (59) synchronize to $\boldsymbol{y}_0$ in (60) and hence the direct term of DG output voltages v_{odi} synchronizes to v_{ref}, if the feedback gain K is chosen as

$$K = R^{-1}B^T P_1, \tag{66}$$

where P_1 is the unique positive-definite solution of the control algebraic Riccati equation (ARE)

$$A^T P_1 + P_1 A + Q - P_1 B R^{-1} B^T P_1 = 0, \tag{67}$$

and

$$c \geq \frac{1}{2\lambda_{min}}, \tag{68}$$

where $\lambda_{min} = min_{i\in N} Re(\lambda_i)$, where $\lambda_i (i \in \{1,2,\dots,N\})$ are the eigenvalues of $L + B$.

Distributed Secondary Voltage Control: Feedback linearization

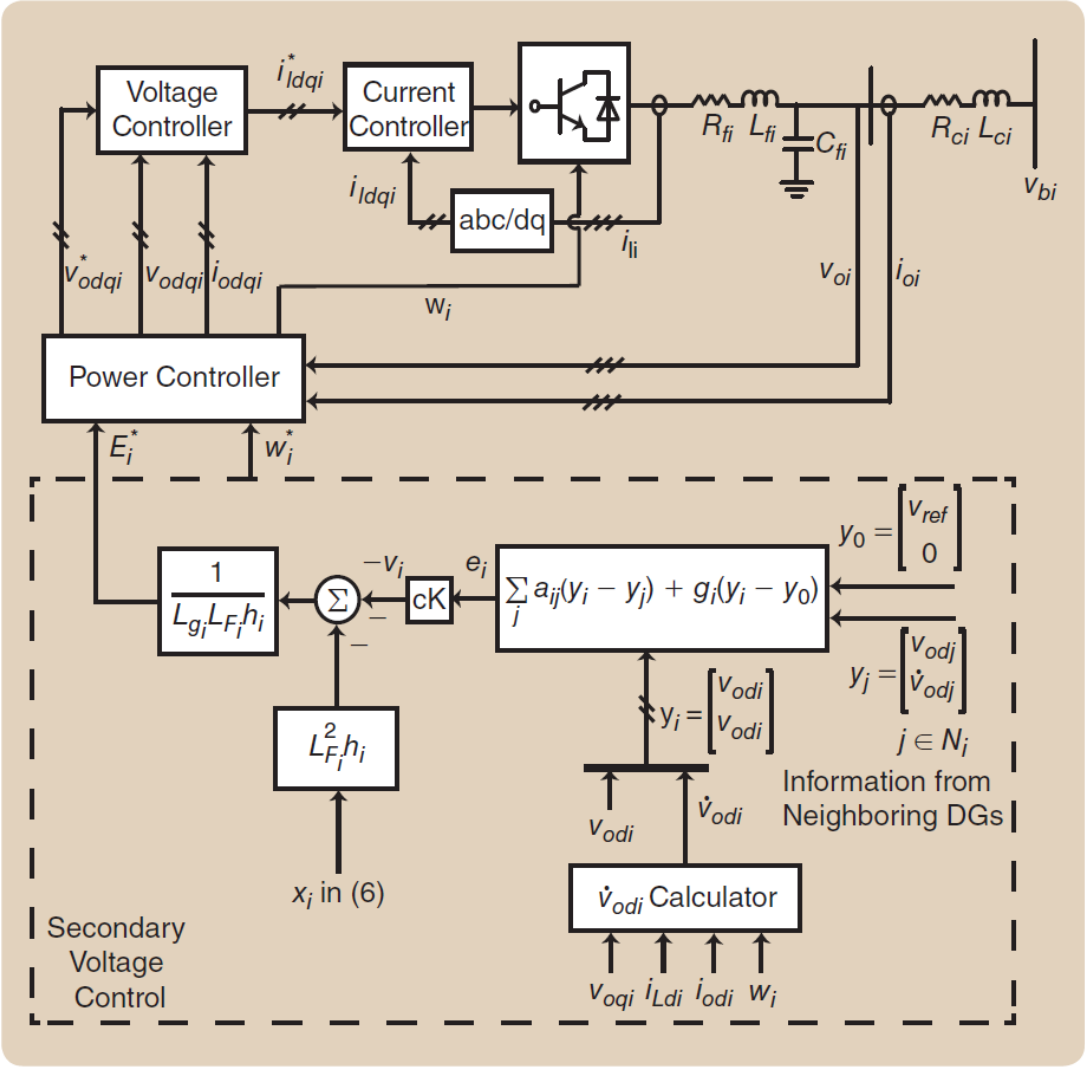

Fig. 30 The block diagram of the proposed secondary voltage control. The secondary voltage control at each distributed generator (DG) only requires its own and neighboring DGs' terminal voltage amplitude and first derivative [20].

Distributed Secondary Voltage Control: Feedback linearization

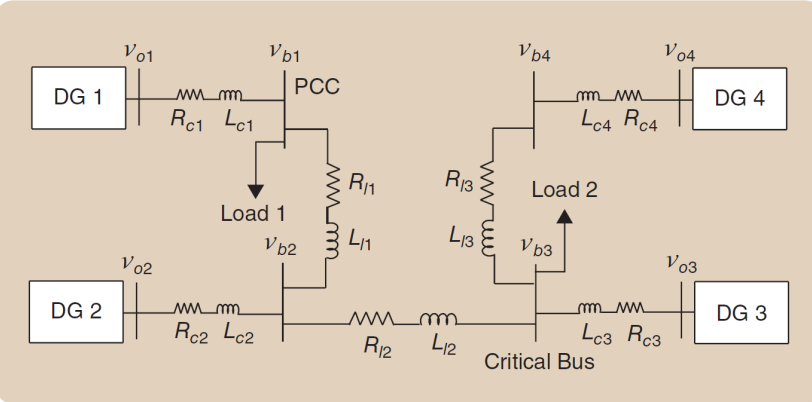

Fig. 31 Single-line diagram of the microgrid test system.

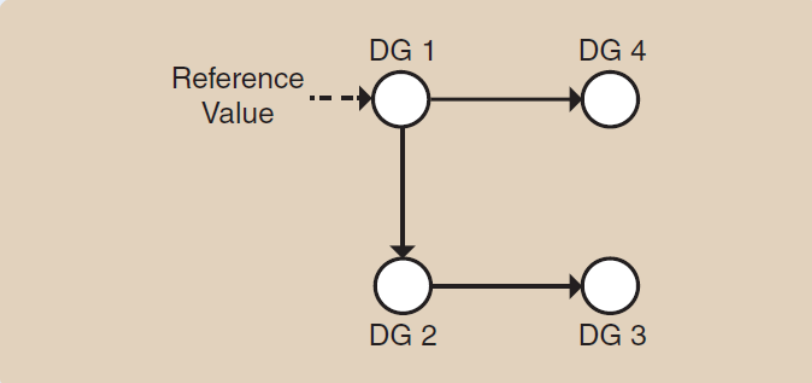

Fig. 32 Topology of the communication digraph.

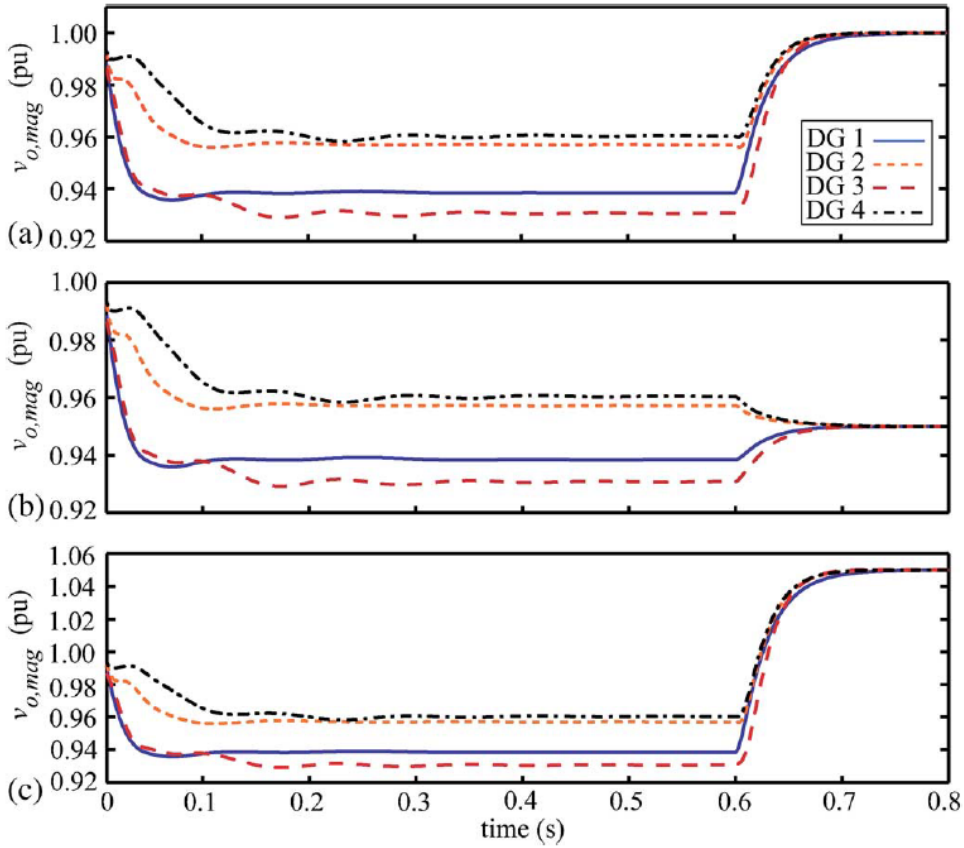

Fig. 33 DG output voltage magnitudes for Case B: (a) when $v_{ref} = 1$ p.u., (b) when $v_{ref} = 0.95$ p.u., and (c) when $v_{ref} = 1.05$ p.u.. [20].

[20] A. Bidram, F. L. Lewis and A. Davoudi, "Distributed Control Systems for Small-Scale Power Networks: Using Multiagent Cooperative Control Theory," in IEEE Control Systems Magazine, vol. 34, no. 6, pp. 56-77, Dec. 2014.

Distributed Secondary Frequency Control: Feedback linearization

The secondary frequency control is similar to that of voltage control. The primary frequency control is considered,

$$\omega_i = \omega_i^* - D_{Pi}P_i, \tag{69}$$

where ω_i^* is the primary frequency control reference and Dpi is the frequency-active power droop coefficient. The secondary frequency control chooses ω_i^* such that the angular frequency of each DG, ω_i, synchronizes to the nominal angular frequency, ω_{ref}, that is, $2\pi \times 50$ or $2\pi \times 60$ rad/s. Once the secondary frequency control is applied, the DG output powers are allocated according to the same pattern used for primary control.

Differentiating the frequency-droop characteristic in (69) yields

$$\dot{\omega}_i^* = \dot{\omega}_i + D_{Pi}\dot{P}_i = u_i, \tag{70}$$

The auxiliary controls u_i are chosen as

$$u_i = -c_f \left[\sum_{j \in N_i} a_{ij}(\omega_i - \omega_j) + b_i(\omega_i - \omega_{ref}) + \sum_{j \in N_i} a_{ij}(D_{Pi}P_i - D_{Pj}P_j) \right], \tag{71}$$

where $c_f \in \mathbb{R}$ is the coupling gain. It is assumed that the pinning gain $b_i \geq 0$ is nonzero for only one DG that has the reference frequency ω_{ref}.

Distributed Secondary Frequency Control: Feedback linearization

The block diagram of the secondary frequency control based on the distributed cooperative control is shown in Figure 12. As seen in this figure, the control input ω_i^* to the primary control level is

$$\omega_i^* = \int u_i dt. \tag{72}$$

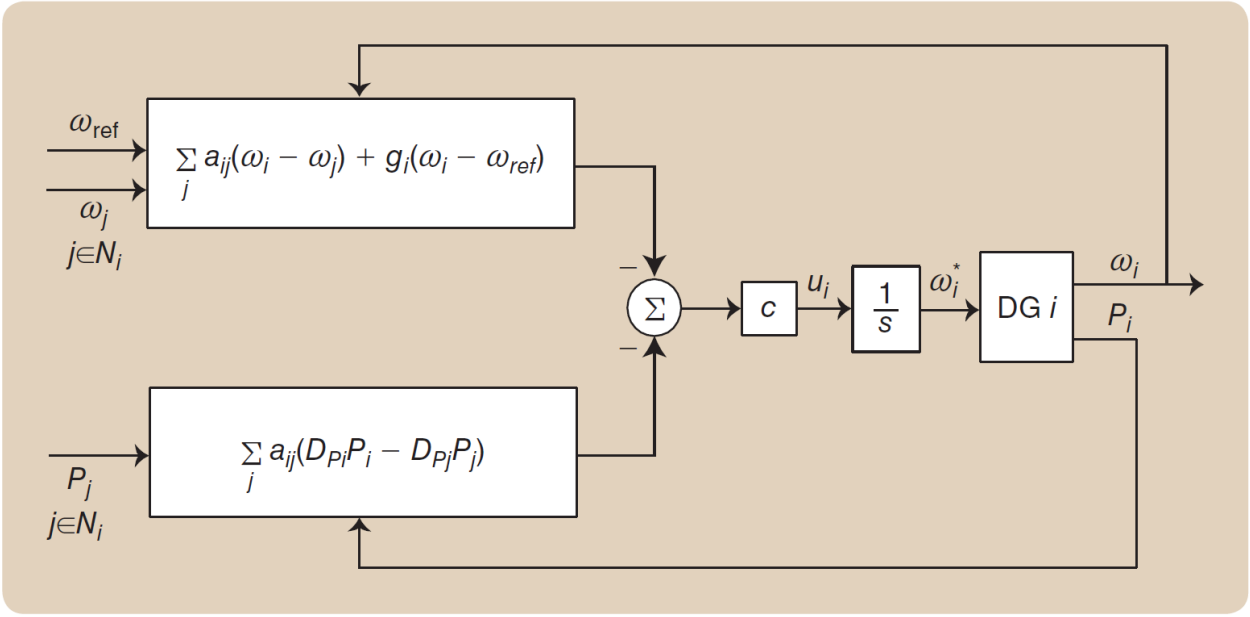

Fig. 34 The block diagram of the distributed secondary frequency control. The secondary frequency control at each distributed generator (DG) only requires its own frequency and active power, and the frequency and active power of neighboring DGs on the communication network. [20].

References

[1] M. Rasheduzzaman, J. A. Mueller, and J. W. Kimball, “An accurate small-signal model of inverter-dominated islanded microgrids using dq reference frame,” IEEE J. Emerg. Sel. Topics Power Electron., vol. 2, no. 4, pp. 1070–1080, Dec. 2014.
[2] M. Rasheduzzaman, J. A. Mueller, and J. W. Kimball, Rasheduzzaman. "Reduced-order small-signal model of microgrid systems." IEEE Transactions on Sustainable Energy 6.4 (2015): 1292-1305.
[3] P. V. Kokotovic, “A Riccati equation for block-diagonalization of ill-conditioned systems,” IEEE Trans. Autom. Control, vol. 20, no. 6, pp. 812–814, Dec. 1975.
[4] A. Bidram and A. Davoudi, "Hierarchical Structure of Microgrids Control System," in *IEEE Transactions on Smart Grid*, vol. 3, no. 4, pp. 1963-1976, Dec. 2012.
[5] M. J. Ryan, W. E. Brumsickle, and R. D. Lorenz, “Control topology options for single-phase UPS inverters,” IEEE Trans. Ind. Appl., vol. 33, pp. 493–501, Mar./Apr. 1997.
[6] G. Escobar, P. Mattavelli, A. M. Stankovic, A. A. Valdez, and J. L. Ramos, “An adaptive control for UPS to compensate unbalance and harmonic distortion using a combined capacitor/load current sensing,” IEEE Trans. Ind. Appl., vol. 54, pp. 839–847, Apr. 2007.
[7] A. Hasanzadeh, O. C. Onar, H. Mokhtari, and A. Khaligh, “A proportional-resonant controller-based wireless control strategy with a reduced number of sensors for parallel-operated UPSs,” IEEE Trans. Power Del., vol. 25, pp. 468–478, Jan. 2010.
[8] M. Prodanović and T. C. Green, “High-quality power generation through distributed control of a power park microgrid,” IEEE Trans. Ind. Electron., vol. 53, pp. 1471–1482, Oct. 2006.
[9] E. Rokrok and M. E. H. Golshan, “Adaptive voltage droop method for voltage source converters in an islanded multibus microgrid,” IET Gen., Trans., Dist., vol. 4, no. 5, pp. 562–578, 2010.
[10] M. C. Chandorkar, D. M. Divan, and R. Adapa, “Control of parallel connected inverters in standalone AC supply systems,” IEEE Trans. Ind. Appl., vol. 29, pp. 136–143, Jan./Feb. 1993.
[11] C. K. Sao and W. Lehn, “Autonomous load sharing of voltage source converters,” IEEE Trans. Power Del., vol. 20, pp. 1009–1016, Apr. 2005.

References

[12] C. K. Sao and W. Lehn, “Control and power management of converter fed microgrids,” IEEE Trans. Power Syst., vol. 23, pp. 1088–1098, Aug. 2008.
[13] Y. Li and Y. W. Li, “Power management of inverter interfaced autonomous microgrid based on virtual frequency-voltage frame,” IEEE Trans. Smart Grid, vol. 2, pp. 30–40, Mar. 2011.
[14] W. Yao,M. Chen, J. Matas, J. M. Guerrero, and Z. Qian, “Design and analysis of the droop control method for parallel inverters considering the impact of the complex impedance on the power sharing,” IEEE Trans. Ind. Electron., vol. 58, pp. 576–588, Feb. 2011.
[15] J. M. Guerrero, L. G. D. Vicuna, J. Matas, M. Castilla, and J. Miret, “Output impedance design of parallel-connected UPS inverters with wireless load-sharing control,” IEEE Trans. Ind. Electron., vol. 52, pp. 1126–1135, Aug. 2005.
[16] A. Tuladhar, H. Jin, T. Unger, and K. Mauch, “Control of parallel inverters in distributed AC power systems with consideration of line impedance effect,” IEEE Trans. Ind. Appl., vol. 36, pp. 131–138, Jan./Feb. 2000.
[17] U. Borup, F. Blaabjerg, and P. N. Enjeti, “Sharing of nonlinear load in parallel-connected three-phase converters,” IEEE Trans. Ind. Appl., vol. 37, pp. 1817–1823, Nov./Dec. 2001.
[18] A. Bidram, et al. "Secondary control of microgrids based on distributed cooperative control of multi-agent systems." IET Generation, Transmission & Distribution 7.8 (2013): 822-831.
[19] F. Katiraei, M. R. Iravani, and P. W. Lehn, “Microgrid autonomous operation during and subsequent to islanding process,” IEEE Trans. Power Del., vol. 20, pp. 248–257, Jan. 2005.
[20] A. Bidram, F. L. Lewis and A. Davoudi, "Distributed Control Systems for Small-Scale Power Networks: Using Multiagent Cooperative Control Theory," in IEEE Control Systems Magazine, vol. 34, no. 6, pp. 56-77, Dec. 2014.

Thank you!